

Research Articles: Neurobiology of Disease

High dietary fat consumption impairs axonal mitochondrial function *in vivo*

<https://doi.org/10.1523/JNEUROSCI.1852-20.2021>

Cite as: J. Neurosci 2021; 10.1523/JNEUROSCI.1852-20.2021

Received: 15 July 2020

Revised: 11 February 2021

Accepted: 15 March 2021

This Early Release article has been peer-reviewed and accepted, but has not been through the composition and copyediting processes. The final version may differ slightly in style or formatting and will contain links to any extended data.

Alerts: Sign up at www.jneurosci.org/alerts to receive customized email alerts when the fully formatted version of this article is published.

1 **High dietary fat consumption impairs axonal mitochondrial function *in vivo***

2 Abbreviated title: High-fat diet impairs axon mitochondrial function

3 Marija Sajic,^{1,*‡} Amy E. Rumora,^{2,‡} Anish A. Kanhai,¹ Giacomo Dentoni,¹ Sharlini Varatharajah,¹
4 Caroline Casey,¹ Ryan D. R. Brown,¹ Fabian Peters,¹ Lucy M. Hinder,² Masha G. Savelieff,³ Eva
5 L. Feldman,² and Kenneth J. Smith¹

6 ¹Department of Neuroinflammation, UCL Queen Square Institute of Neurology, Queen Square,
7 London, WC1N 3BG

8 ²Department of Neurology, University of Michigan, Ann Arbor, MI 48109, USA

9 ³NeuroNetwork for Emerging Therapies, University of Michigan, Ann Arbor, MI 48109, USA

10 *Correspondence: m.sajic@ucl.ac.uk (M.S.)

11 ‡Marija Sajic and Amy E. Rumora contributed equally.

12 **Number of pages:** 44 pages

13 **Number of figures:** (main: 7)

14 **Number of tables:** (main: 0)

15 **Number of extended data figures:** (main: 8)

16 **Number of extended data tables:** (main: 0)

17 **Word count:** (abstract: 249 words) and (introduction: 645 words) and (discussion: 1,500 words)

18 **Conflict of interest statement:** The authors declare no competing financial interests.

19 **Acknowledgments:** This work was supported by the Leducq Foundation (to M.S. and K.J.S.),
20 the National Institutes of Health (NIH 1T32DK101357, F32DK112642 and 1K99DK119366 to
21 A.E.R.; R21NS102924 and R24DK082841 to E.L.F.), the Novo Nordisk Foundation
22 (NNF14OC0011633 to E.L.F.), and the NeuroNetwork for Emerging Therapies. The complex

23 lipid analysis was completed by the University of Cincinnati Medical Center MMPC supported by
24 the U24 DK059630 grant. The authors also thank Dr. Oliver Griesbeck, Max Planck Institute, for
25 the Tn-XXL mice; Dr. Stacey Sakowski Jacoby, University of Michigan, for expert editorial
26 assistance; Ms. Faye E. Mendelson, University of Michigan, for technical assistance; and Mr.
27 John Hayes, University of Michigan, for assistance with data visualization.

28 **Abstract**

29 Peripheral neuropathy (PN) is the most common complication of prediabetes and diabetes. PN
30 causes severe morbidity for type 2 diabetes (T2D) and prediabetes patients, including limb pain
31 followed by numbness resulting from peripheral nerve damage. PN in T2D and prediabetes is
32 associated with dyslipidemia and elevated circulating lipids; however, the molecular
33 mechanisms underlying PN development in prediabetes and T2D are unknown. Peripheral
34 nerve sensory neurons rely on axonal mitochondria to provide energy for nerve impulse
35 conduction under homeostatic conditions. Models of dyslipidemia *in vitro* demonstrate
36 mitochondrial dysfunction in sensory neurons exposed to elevated levels of exogenous fatty
37 acids. Herein, we evaluated the effect of dyslipidemia on mitochondrial function and dynamics in
38 sensory axons of the saphenous nerve of a male high-fat diet (HFD)-fed murine model of
39 prediabetes to identify mitochondrial alterations that correlate with PN pathogenesis *in vivo*. We
40 found that the HFD decreased mitochondrial membrane potential (MMP) in axonal mitochondria
41 and reduced the ability of sensory neurons to conduct at physiological frequencies. Unlike
42 mitochondria in control axons, which dissipated their MMP in response to increased impulse
43 frequency (from 1 to 50 Hz), HFD mitochondria dissipated less MMP in response to axonal
44 energy demand, suggesting a lack of reserve capacity. The HFD also decreased sensory
45 axonal Ca^{2+} levels and increased mitochondrial lengthening and expression of PGC1 α , a
46 master regulator of mitochondrial biogenesis. Together, these results suggest that mitochondrial
47 dysfunction underlies an imbalance of axonal energy and Ca^{2+} levels and impairs impulse
48 conduction within the saphenous nerve in prediabetic PN.

49

50 **Significance Statement**

51 Diabetes and prediabetes are leading causes of peripheral neuropathy (PN) worldwide. PN has
52 no cure, but development in diabetes and prediabetes is associated with dyslipidemia, including

53 elevated levels of saturated fatty acids. Saturated fatty acids impair mitochondrial dynamics and
54 function in cultured neurons, indicating a role for mitochondrial dysfunction in PN progression;
55 however, the effect of elevated circulating fatty acids on the peripheral nervous system *in vivo* is
56 unknown. In this study, Sajic et al. identify early pathogenic events in sensory nerve axons of
57 mice with high-fat diet-induced PN, including alterations in mitochondrial function, axonal
58 conduction, and intra-axonal calcium, that provide important insight into potential PN
59 mechanisms associated with prediabetes and dyslipidemia *in vivo*.

60 **Introduction**

61 Diabetes and prediabetes incidence is rising at alarming rates. In 2019, ~463 million people
62 globally had diabetes, with a projected increase to ~700 million by 2045 (Saeedi et al., 2019).
63 Peripheral neuropathy (PN), the most prevalent prediabetic and diabetic complication, affects
64 ~50% of type 2 diabetes (T2D) patients and 33% of prediabetic patients in the United States
65 (Feldman et al., 2019). Characterized by nerve damage, PN manifests as pain or sensory loss
66 starting in the feet and then the hands in a “stocking and glove” pattern. At end-stages,
67 complete loss of sensation in peripheral tissues results in morbidity, including gait problems,
68 foot ulcerations, and lower limb amputation. Early attempts to prevent PN in prediabetes and
69 T2D patients focused on glycemic control alone, which was only marginally successful
70 (Callaghan et al., 2012). As the increased prevalence of prediabetes and T2D is associated with
71 obesity and high-fat “Western” diets, saturated fatty acids (SFAs) and dyslipidemia likely play
72 important roles in PN progression (Eid et al., 2019). Indeed, recent clinical studies have
73 correlated PN progression with the metabolic syndrome and dyslipidemia in both prediabetes
74 and T2D, independent of glycemic control (Callaghan et al., 2016b; Callaghan et al., 2016a;
75 Callaghan et al., 2018; Callaghan et al., 2020).

76 Although overwhelming preclinical and clinical evidence indicate that a SFA-rich diet
77 correlates with PN development (Savelieff et al., 2020), molecular mechanisms remain poorly
78 understood. Dorsal root ganglion (DRG) neurons, the primary sensory neurons affected by PN,
79 have axons up to a meter long in humans and thus require long-distance axonal transport of
80 functional mitochondria to satisfy distal ATP demands and maintain adequate Ca^{2+} buffering
81 (Sajic, 2014). Elevated long-chain SFA levels impair mitochondrial metabolism (Schonfeld and
82 Wojtczak, 2016), and we demonstrated that exogenous long-chain SFAs reduce mitochondrial
83 membrane potential (MMP), bioenergetics capacity, ATP production, and motility of axonal
84 mitochondria in cultured DRG neurons, while physiological glucose had no effect (Rumora et al.,

85 2018; Rumora et al., 2019a). Since PN is characterized by distal-to-proximal axonal
86 degeneration, we hypothesized that SFA-induced impairment in mitochondrial function and
87 transport *in vivo* are an important cause of PN progression.

88 Mitochondrial function has been investigated *in vitro* (Feldman et al., 2017), and in *in vivo*
89 models where myelination affects mitochondrial function and dynamics (Zhang et al., 2010;
90 Ohno et al., 2011; Sajic et al., 2013). *In vitro*, MMP and mitochondrial motility are constantly
91 influenced by growth cues from neurite outgrowth in culture (Morris and Hollenbeck, 1993;
92 Chada and Hollenbeck, 2004), but these cues are missing *in vivo* in healthy adult animals.
93 Cultured or *ex vivo* preparations also lack a perfused vasculature to ensure physiological
94 nutrient and oxygenation levels (Sajic, 2014). To overcome these constraints and validate our *in*
95 *vitro* findings (Rumora et al., 2018; Rumora et al., 2019a), we examined mitochondria *in vivo*
96 within the homeostatically-regulated environment of adult, electrically active saphenous nerve
97 axons in a high-fat diet (HFD)-induced prediabetes mouse model. The HFD chow contains 45%
98 lard, mimicking a “Western” SFA-rich diet (O’Brien et al., 2014). HFD-fed mice recapitulate
99 salient features of prediabetes, including impaired glucose tolerance, obesity, and neuropathy,
100 and they develop electrophysiological and histological characteristics of human PN, *e.g.*,
101 reduced sensory and motor nerve conduction velocities and decreased intraepidermal nerve
102 fiber density (IENFD) (O’Brien et al., 2014), making it a useful model for evaluating PN
103 mechanisms.

104 We report that mitochondrial transport in saphenous nerve axons of prediabetic HFD mice is
105 intact *in vivo*. However, axonal mitochondria suffer from significantly reduced MMP, which does
106 not dissipate in response to physiological increases in axonal energy demand in HFD mice
107 versus control mice. These changes also associate with significant decreases in intra-axonal
108 calcium levels ($[Ca^{2+}]_i$) and lower expression of PGC1 α , a master regulator mitochondrial
109 biogenesis, in prediabetic versus control mice. These results suggest that partial MMP loss and

110 reduced $[Ca^{2+}]_i$ play important roles in regulating sensory neuron axonal impulse conduction in
111 peripheral nerves of prediabetic HFD mice with PN.

112

113 **Materials and methods**

114 **Animals**

115 All experiments were carried out under the United Kingdom (UK) 1986 Animals (Scientific
116 Procedures) Act, the UK 2006 Animal Welfare Act, and the European Directive 2010/63/EU. All
117 experiments were approved by the institutional ethics committee and followed the ARRIVE
118 guidelines. Mouse strains used in this study included positive and negative littermates of
119 genetically modified Tn-XXL mice (Mank et al., 2008) and B6.CG-Tg(Thy1-
120 CFP/COX8A)S2Lich/J mice (The Jackson Laboratories, catalog # 007967). All mice were
121 housed in individually ventilated cages with a maximum of 5 mice per cage that were provided
122 with bedding, nesting material, playing tunnels, and wood blocks. Mice had access to food, as
123 specified in the experimental design, and water *ad libitum*, and were kept on a 12h light/12h
124 dark cycle. At study termination, plasma was collected and submitted to the Cincinnati Mouse
125 Metabolic Phenotyping Center for a complex lipid panel analysis to measure circulating
126 phospholipids, cholesterol, triglycerides, and non-esterified fatty acids. Both male and female
127 mice were also evaluated for sex differences related to food consumption, weight gain,
128 hyperglycemia, glucose tolerance, and tactile hypersensitivity prior to assessment of *in vivo*
129 mitochondrial events. Food consumption was evaluated by measuring the gram amount of food
130 consumed per mouse per day for both male and female mice.

131

132 **Fasting glucose**

133 Blood glucose measurements were performed after overnight fasting, using a commercially
134 available Accu-Check Mobile blood glucose monitor (Roche), from a single, minimally invasive
135 tail puncture.

136

137 **Intraperitoneal glucose tolerance test**

138 The intraperitoneal (i.p.) glucose tolerance test (ipGTT) was performed according to the
139 DiaComp protocol (<https://www.diacomp.org/shared/showFile.aspx?doctypeid=3&docid=11>).
140 Briefly, after the fasting period, mice were weighed, and a baseline blood glucose measurement
141 was obtained, as described above. An intraperitoneal injection of glucose (1 mg/g) (Sigma-
142 Aldrich, UK) was administered, and further blood glucose measurement were acquired 15, 30,
143 60, and 120 min after the i.p. injection.

144

145 **Tactile hypersensitivity**

146 Tactile responses were evaluated as described before (Obrosova et al., 2007). In short, mice
147 were transferred into a clear Plexiglas box with mesh floor, and allowed to acclimatize.
148 Following the acclimatization period, a series of flexible von Frey filaments (NC12775-99, North
149 Coast, USA) were applied to the surface of the hind paws with adequate force to bend the
150 filament for 6 seconds. Paws were stimulated alternately and stimulations were repeated 6
151 times. Short paw withdrawal or paw flinching was classified as a positive response. Stimulation
152 was stopped when > 50% of the 6 stimuli were positive, otherwise, the filament with the next
153 greater force was applied. Tactile response thresholds were calculated with the formula $[(w_1 \times$
154 $r_1) + (w_2 \times r_2) + (w_x \times r_x)]/r_{total}$, with w corresponding to filament weight and r corresponding to
155 number of positive responses for that filament.

156

157 **Experimental design**

158 Mitochondrial dynamics experiments: Cyan fluorescent protein (CFP) transgenic mice (B6.Cg-
159 Tg(Thy1-CFP/COX8A)S2Lich/J, The Jackson Laboratories, catalog # 007967) with constitutive
160 expression in 40-60% of mitochondria were used for imaging mitochondria *in vivo*. Male
161 littermates were randomly assigned to either a control chow diet (Lab Diet 5001 Cat#: 0001319,
162 13% kcal fat) or HFD (Research Diets Cat#: D12451, 45% kcal fat) according to the following
163 regimens: (i) 4-week-old mice fed control or HFD for 16 weeks (4+16 group, aged 20 weeks at
164 experiment termination), (ii) 4-week-old mice fed control or HFD for 36 weeks (4+36 group,
165 aged 40 weeks at experiment termination), or (iii) 24-week-old mice fed control or HFD for 16
166 weeks (24+16, aged 40 weeks at experiment termination). Dietary composition, fatty acid
167 makeup, and energy density of the control diet and HFD chows are detailed in Figure 1-1.
168 Animals were weighed weekly and examined for signs of pain or discomfort.

169

170 Calcium imaging experiments: Tn-XXL transgenic mice, which express a calcium-binding
171 troponin C-based biosensor with two fluorescent probes, citrine and CFP, were used for imaging
172 calcium (Mank et al., 2008). Two experiments were performed. In the first, 9-week-old male
173 littermates were randomly assigned to either a control diet or HFD for 5 weeks (9+5 group, aged
174 14 weeks at experiment termination). In the second, 24-week-old male littermates were
175 randomly assigned to either a control diet or HFD for 16 weeks (24+16 group, aged 40 weeks at
176 experiment termination).

177

178 **Surgical procedure, *in vivo* imaging, and electrophysiology**

179 Animals were terminally anesthetised (urethane; i.p., 1.25 g/kg) (Sigma-Aldrich), the leg was
180 immobilised using a mold made from dental polymer (Examix NDS Monophase Purple, GC

181 America) (Misgeld et al., 2007). The left saphenous nerve was exposed at three locations, at the
182 mid-thigh for confocal imaging, at the groin for the stimulating electrode, and at the ankle for the
183 recording electrode. The left saphenous nerve exposed at mid-thigh was desheathed, as
184 described previously (Sajic et al., 2013), and stained *in situ* with tetramethylrhodamine methyl
185 ester [TMRM (Invitrogen/Thermo Fisher Scientific, UK); 0.5 μ M in artificial cerebrospinal fluid
186 (aCSF) (Harvard Apparatus, Holliston, MA, USA) for 30 min], and the surrounding structures
187 with fluorescein isothiocyanate-conjugated *Griffonia* isolectin B4 (1:20 in sterile saline for 10
188 min) (Sigma-Aldrich), in addition to the constitutive CFP labeling. While the dyes incubated at
189 the mid-thigh, the saphenous nerve was exposed in the groin to create a “well” with the exposed
190 part of the nerve at its bottom. Teflon tape, approximately 2 cm \times 0.5 cm, was placed under the
191 nerve to electrically isolate it from the surrounding muscle. A pair of stimulating platinum wire
192 electrodes was placed under the saphenous nerve, resting on the Teflon tape. The well was
193 then filled with mineral oil to prevent tissue drying. Next, the saphenous nerve was exposed at
194 the ankle to attach the active recording electrode, which was placed directly next to the exposed
195 distal part of the saphenous nerve. A reference needle electrode was inserted into the fifth toe,
196 and a ground electrode was placed in the abdominal muscle. At this stage, the animal was
197 transferred to the confocal microscope (LSM Pascal 710, Zeiss, Germany). Fresh saline was
198 applied to the exposed saphenous nerve at mid-thigh and covered with a glass coverslip sealed
199 with petroleum jelly. Confocal time-lapse and single images were taken using either a Zeiss
200 Apochromat 10x objective (NA 0.3; overview only) or a Zeiss Apochromat Plan 63x oil objective
201 (NA 1.4). The pinhole size was set to 1 AU and time-lapse sequences were recorded at 1
202 frame/s for 100 s. Successive dual-colour CFP / TMRM (405 nm / 543 nm) images were taken
203 to distinguish axonal mitochondria from mitochondria found in other cells. However, time-lapses
204 were based on the TMRM signal alone because of its superior contrast and because repeated
205 CFP imaging causes a prohibitive amount of bleaching. Time-lapse images of mitochondria
206 were taken simultaneously with electrophysiological stimulation and recording. First, a single

207 supramaximal stimulus was delivered at frequencies of 1 Hz and 50 Hz. Sensory compound
208 action potentials (sCAPs) were averaged ($n = 30$) and stored (Sigma 60, Nicolette
209 Technologies). Next, to examine the refractory period of transmission (RPT), two successive
210 supramaximal stimuli were delivered while sequentially increasing the delay between the first
211 and second stimulus in 0.1 ms increments, up to 2.5 ms. sCAPs were averaged ($n = 30$) and
212 stored (Sigma 60, Nicolette Technologies). The amplitudes were measured using Matlab.

213

214 ***In vivo* calcium imaging**

215 Tn-XXL mice were prepared for imaging as described above. However, no dyes were applied to
216 the nerve and images were acquired using a Zeiss Apochromat Plan 63x oil objective (NA 1.4).
217 First, axons of interest were identified by exciting the citrine fluorophore of Tn-XXL directly via a
218 514 nm laser. Next, two 512 x 512 pixel images were taken for every axon: (i) a 'ratiometric'
219 two-channel image with an excitation of 405 nm and detection ranges of 460 nm – 510 nm (for
220 CFP) and 520 nm – 570 nm (for citrine), and (ii) an 'anatomical' image with 514 nm excitation
221 and a broad detection range of 515 nm – 650 nm. Laser settings were constant across all
222 animals. The initial calibration was performed in naïve Tn-XXL animals, which was removed
223 from the microscope stage after visible axons were imaged. Then ionomycin (100 μ M in aCSF)
224 was applied to the nerve for 10 min, a new coverslip was placed over the leg, and imaging was
225 repeated.

226

227 **Tissue collection**

228 After sCAPs and/or images were acquired, mice were perfused transcardially with
229 paraformaldehyde (PFA, 4% in 0.4 M phosphate buffer, pH 7.4) (VWR Chemicals, UK). Sciatic
230 nerves and spinal cord lumbar segments (L3, L4, and L5) were dissected and post-fixed for 2 h

231 (PFA, 4% in 0.4 M phosphate buffer), whereas glabrous and hairy skin were post-fixed
232 overnight. After post-fixation, tissues were transferred to 0.1% sodium azide (VWR Chemicals)
233 in phosphate buffered saline (PBS). A block of hairy skin from the medial side of the foot
234 dorsum, innervated by saphenous nerve, and a block of glabrous skin from the foot plantar
235 innervated by the sciatic nerve were dissected. Skin blocks and spinal cord tissue were
236 separately embedded into paraffin wax. Eight micron sections were cut using a microtome (Leitz
237 1512, Germany), transferred into a water bath (Medlite Tissue Flotation Bath, TFB- 45,
238 Medizintechnik, Germany) set at a temperature of 40 °C, mounted onto slides (Superfrost,
239 Thermo Scientific, UK), and left to air-dry overnight.

240

241 **Immunohistochemistry**

242 To assess PGC1 α expression in DRGs or skin intraepidermal nerve fibre density, sections were
243 incubated with anti-PGC1 α (Abcam, ab54481, RRID:AB_881987) and anti- β -III-tubulin (Abcam,
244 ab78078, RRID:AB_2256751) antibodies, respectively. First, the slides were deparaffinised by
245 incubating in xylene (VWR Chemicals) for 5 min, xylene/100% ethanol 1:1 for 3 min, and then 3
246 min each in serial ethanol dilutions: 100%, 90%, 70%, 50% (VWR Chemicals). Slides were
247 rinsed in distilled water for 3 min followed by cold acetone (VWR Chemicals) for 5 min. After
248 deparaffinization, the slides were washed twice in PBS for 5 min. Antigen retrieval was
249 performed by heating slides to boiling in 10% citrate solution (pH 6; Dako, UK) and then
250 transferring to an oven at 40 °C for 40 minutes. The slides were then rinsed in distilled water,
251 followed by two washes in PBS-T (PBS with 0.2% Triton X-100, Sigma-Aldrich). Slides were
252 then blocked in 5% rabbit serum in PBS-T (Vector Laboratories Inc., UK) for 1 h in a humidified
253 chamber at room temperature. The serum was removed with a Pasteur pipette, and the primary
254 antibodies, polyclonal rabbit anti-PGC1 α (1:600) and monoclonal mouse anti-neuronal β -III
255 tubulin (1:1,000) diluted in 2% blocking solution were applied overnight at 4 °C. The next day,

256 the slides were washed twice in PBS and once in distilled water, each for 5 min. The goat anti-
257 rabbit AlexaFluor 546 (Invitrogen Thermo Fisher Scientific, catalog # A11010, RRID: 2534077)
258 or goat anti-mouse AlexaFluor 647 (Invitrogen Thermo Fisher Scientific, catalog # 32728, RRID:
259 AB_2633277), were added to their respective primary for 1 h in the dark. Next, the slides were
260 washed three times in PBS for 5 min and then rinsed with distilled water. The slides were air
261 dried in the dark. Coverslips were mounted using 4',6-diamidino-2-phenylindole (DAPI)
262 fluoromount (Vectashield, Vector Laboratories, UK) and sealed using nail varnish. Additionally,
263 in processing tissue for DRGs, a 70% methanol (VWR Chemicals) pre-treatment step was
264 carried out after deparaffinization. Also, two rounds of incubation in 1% sodium borohydrite
265 (Sigma-Merck) for 5 min each were carried out after antigen retrieval, followed by incubation in
266 blocking solution with 20% rabbit serum. All sections were immunolabeled in the same session.
267 For image acquisition, fluorescence emission was recorded through a 10x/0.3, Zeiss EC Plan
268 Neofluar 10x/0.3 Ph2 or Plan-Apochromat 63x/1.4 Oil Ph3 (Zeiss) objective lens. All images
269 were acquired with the following settings: beam-splitter HFT 488/543; filter BP 505–570, argon
270 laser irradiation at 488 nm and filter LP 585 helium neon laser irradiation at 543 nm. First, tile
271 scans were carried out using Zeiss EC Plan Neofluar 10x/0.3 Ph2 magnification using blue
272 (DAPI, 405 nm) and red (AlexaFluor546, 565 nm) channels. For images of β -III-tubulin labeled
273 hairy and glabrous skin sections, Z-stack images from five, randomly chosen, non-overlapping
274 positions were acquired using Zeiss EC Plan Neofluar 40x/0.75 Ph2 (water) objective (Zeiss,
275 Germany) and ZEN black acquisition software (Zeiss). If the image did not appear to be
276 uniformly labeled across the field of view, the next random area was chosen for image
277 acquisition. Each Z-stack contained ten images, each at 1 μ m thickness. For images of PGC1 α -
278 labeled DRGs, Z-stacks were taken in the same way, while using the Zeiss Plan-Apochromat
279 65x/1.40 (oil) Ph3 objective. Care was taken not to saturate pixel intensity during image
280 acquisition. Tissue dissection, embedding, sectioning, immunolabeling, and image acquisition
281 and image analysis were performed in a blinded fashion.

282

283 **Western blot analysis**

284 VDAC1/2, MFN2, and PGC1 α protein expression level was evaluated in the L1-L5 lumbar DRG
285 or sural nerves from a separate cohort of mice fed either standard diet (Research Diets,
286 D12450B) or 45% HFD (Research Diets, D12451) from 4-36 weeks of age. Western blotting
287 was conducted per our previous study (Vincent et al., 2010). Briefly, L1-L5 DRG or sural nerve
288 from each mouse were pulverized with a pestle, resuspended in 50 μ l of RIPA lysis buffer
289 (Sigma-Aldrich) with protease inhibitors (Roche), and evaluated for protein concentration. A total
290 of 10 μ g of protein/lane were separated on a 12.5% polyacrylamide gel and transferred to a
291 nitrocellulose membrane. Antibodies against PGC1 α (Abcam, catalog # ab188102), MFN2
292 (Protein Tech, catalog # 12186-1-AP, RRID: AB_2266320), and VDAC1/2 (Protein Tech,
293 catalog # 10866-1-AP, RRID: RRID:AB_2257153) were used to detect proteins. Membranes
294 were then washed and probed for loading controls tubulin (Abcam, catalog # ab6160, RRID:
295 AB_305328) and YWHAZ (ProteinTech, catalog #1 4881-1-AP, RRID: AB_2218248).

296

297 ***In vivo* confocal image analyses**

298 Mitochondrial movement was analyzed as described previously (Sajic et al., 2013) using the
299 *Difference Tracker* plugin for ImageJ Fiji (SciJava) (Andrews et al., 2010). Mitochondrial size
300 was evaluated in single images from a minimum of 5 axons from 5 or more non-overlapping
301 regions totaling at least 25 axon regions analyzed per mouse. Each single image showed 50-
302 100 mitochondria, which were analyzed by the Analyse Particle and Measure plugins for
303 ImageJ, using the blue (CFP) channel, as described previously (Sajic et al., 2013). For the
304 analysis of mitochondrial membrane potential, TMRM intensity was measured separately for
305 every mitochondrion relative to its local background. First, the foreground TMRM pixels were

306 identified from overlap with CFP pixels to identify axonal mitochondria. The median intensity of
307 all foreground TMRM pixels of the particle was measured in ImageJ. Next, a local background
308 selection was created containing all pixels within a 3-pixel radius around the mitochondrion of
309 interest which were not part of, or immediately adjacent to, another mitochondrion, and the
310 median intensity of these particles was calculated. The final intensity of a particle was defined
311 as the median foreground intensity divided by the median background intensity. For analyzing
312 $[Ca^{2+}]_i$, image analysis was performed using Matlab (MathWorks). First, all images were filtered
313 using a 3x3 pixel median filter to reduce noise. Individual axons were extracted by manually
314 selecting a rough axon outline. Then, all pixels of interest were selected by thresholding the
315 anatomical (citrine-only) image. For each pixel of interest, the ratio of citrine to CFP in the
316 ratiometric image was calculated. For the images of immunolabeled skin and DRG sections, Z-
317 stacks were collapsed using Zen Black imaging software, which were opened in ImageJ. For the
318 β -III tubulin labeled images, dermis and epidermis in each image were carefully manually
319 selected and the area measured using the *Measure* plugin for ImageJ. The images were then
320 carefully thresholded to ensure that the resulting image faithfully represented the original image.
321 The number of labeled pixels was determined using the *Measure* plugin for ImageJ and
322 expressed per normalised area unit. For the analysis of PGC1 α labeling in DRGs, and β -III
323 tubulin in the skin, three cells in each field of view, with a minimum three fields of view per
324 animal, were randomly chosen from the collapsed Z-stacks. The cell area was carefully outlined
325 and measured using ImageJ. Images were carefully thresholded to ensure that the resulting
326 image faithfully reproduced the original image, and areas of PGC1 α and β -III tubulin labeling
327 were measured again, and expressed as % of the cell or skin area, respectively.

328

329 **Data analysis**

330 Prior to all statistical analyses, the data were tested for normality of distribution using D'Agostino
331 and Pearson normality test with Prism v5 (GraphPad Software). Differences between groups in
332 weight, food consumption, ipGTT, hyperglycemia, tactile hypersensitivity, and all parameters of
333 mitochondrial dynamics and size, and amplitudes of second response in RPT, were calculated
334 using two-way ANOVA with Bonferroni's multiple comparison tests. Two-tailed Student's t-test
335 was used for analyzing differences in terminal blood glucose, MMP, and loss of amplitude after
336 1 h conduction at 50 Hz in HFD versus control mice. Mann-Whitney test was applied to analyze
337 differences in $[Ca^{2+}]_i$ in HFD 9+5 mice and PGC1 α and β -III tubulin coverage. Finally, Kruskal-
338 Wallis test was used to analyze differences between groups in $[Ca^{2+}]_i$ in mice fed HFD for 16
339 weeks starting from 24 weeks of age. An ordinary one-way ANOVA was used to evaluate
340 complex lipid panel data. A two-tailed unpaired t-test was used to assess VDAC1/2, MFN2, and
341 PGC1 α protein expression level in DRG and sural nerves. Parametric data are presented as
342 mean \pm standard error of the mean, whereas non-parametric data, or data that did not follow a
343 normal distribution, are presented as median \pm interquartile range. A p-value < 0.05 was
344 considered statistically significant.

345

346 **Results**

347 **HFD mice exhibit weight gain and impaired glucose tolerance**

348 We examined the effect of HFD on mitochondrial trafficking and function *in vivo* in three
349 experimental groups of mice fed a HFD (45% calories from fat), compared to their respective
350 controls. The first and second groups consisted of "young" mice fed a short- (16 weeks) or long-
351 term (36 weeks) diet, starting at 4 weeks of age, *i.e.*, HFD 4+16 and HFD 4+36 groups,
352 respectively (Figure 1, top). The third group consisted of "older" mice fed short-term (16 weeks)
353 HFD starting from 24 weeks of age (HFD 24+16 group). Corresponding control littermates
354 received control diet (13% calories from fat) for the same duration as their HFD counterparts.

355 HFD mice gained significantly more weight than their control counterparts (Figures 1A-1C).
356 Furthermore, mice from the HFD 4+36 and 24+16 groups developed pronounced hyperglycemia
357 compared to control mice (Figures 1B' and 1C'), whereas glucose tolerance was impaired
358 across all HFD groups (Figures 1A''-1C''). Both HFD and control mice consumed the same
359 amount of food per day, suggesting that the changes to body weight and hyperglycemia are
360 related to diet composition rather than differences in food intake (Figure 1-2). We next assessed
361 the effect of HFD on circulating lipids. Compared to control mice, HFD 4+36 mice had elevated
362 plasma cholesterol and phospholipids levels, but no differences in triglycerides and non-
363 esterified fatty acid (NEFA) levels (Figures 1D-1G). Finally, we evaluated the PN phenotype by
364 quantifying IENFD, which was reduced in glabrous skin of HFD versus control mice (Figure 1-3).
365 Our combined findings show that HFD mice recapitulate metabolic dysfunction in prediabetic
366 patients.

367 An additional cohort of HFD female mice developed hyperglycemia and gained a similar
368 amount of weight to HFD male mice (Figure 1-2), although HFD females had a higher percent
369 increase in body weight versus HFD males starting at 22 weeks. Male and female mice
370 displayed similar tactile hypersensitivity at 20 and 40 weeks, when *in vivo* mitochondrial
371 dynamics were measured, although development was slightly delayed in females (Figure 1-2).
372 Therefore, *in vivo* mitochondrial analyses were only performed in male mice.

373

374 **HFD mice do not exhibit impaired mitochondrial transport in saphenous nerve axons *in***
375 ***vivo***

376 Terminal mitochondrial transport was examined in adult, electrically active, myelinated
377 saphenous nerve axons *in vivo* (Figure 1, top). In this transgenic mouse, about 40 to 60% of
378 axonal mitochondria constitutively express CFP (CFP⁺, Figures 2A and 2B) (Sajic et al., 2013).
379 Nerves were also stained *in situ* with TMRM, a cationic dye that accumulates in mitochondria in

380 proportion to their MMP, staining them red. CFP⁺, unpolarized mitochondria (do not stain with
381 TMRM) will appear cyan, whereas CFP⁺, polarized mitochondria (stain with TMRM) will appear
382 magenta, pink, or white. Unpolarized mitochondria that do not express CFP (CFP⁻) will not be
383 visible, whereas polarized, CFP⁻ mitochondria will be red. At the experimental endpoint, we
384 used time-lapse confocal microscopy to track CFP (axonal mitochondria; non-axonal
385 mitochondria do not express CFP) and TMRM (polarized) labeled motile mitochondria (Movies 1
386 and 2).

387 Sham-stimulated axons, that are presumed to be electrically silent, had a significantly
388 greater number of motile mitochondria in both anterograde and retrograde directions in HFD
389 4+16 mice than corresponding controls (Figure 2C), while other parameters of mitochondrial
390 motility and size were similar. We then analyzed mitochondrial transport in mice fed long-term
391 HFD (4+36 mice, Figure 2D), or in older mice fed the short-term HFD (24+16 mice, Figure 2E,
392 Movies 1 and 2). In addition, in order to mimic physiological axonal activity in live animals, we
393 electrically stimulated saphenous nerve axons at either low (1 Hz) or high (50 Hz) frequency
394 during imaging. Electrical stimulation places an energy demand on axons and, thus,
395 mitochondria mobilize in response. However, regardless of the impulse load on the axons, we
396 found no difference in the number of motile mitochondria between the groups (Figures 2D and
397 2E). Detailed analysis showed that HFD 4+36 mice (Figure 2D) exhibited a significant increase
398 in the *size* of anterogradely transported mitochondria in nerves conducting at 50 Hz, and in the
399 *average speed* of retrogradely transported mitochondria in nerves conducting at 1 Hz, in
400 comparison with controls. Also, in HFD 24+16 mice (Figure 2E), the *average speed* of
401 anterograde mitochondrial transport was significantly higher than in control nerves, at both 1
402 and 50 Hz, and the anterograde *maximal speed* of mitochondrial transport was significantly
403 higher versus controls at only 1 Hz. Overall, however, our results indicate that, in contrast to our
404 expectations from *in vitro* data (Rumora et al., 2018; Rumora et al., 2019a), prediabetic mice do

405 not exhibit impaired mitochondrial transport along saphenous nerve axons *in vivo*. Although
406 there was a small increase in the number, size, and speed of mitochondria in some HFD
407 groups, it was not sufficiently pronounced to affect overall axonal mitochondrial transport.

408

409 **HFD mice exhibit increased stationary mitochondrial size in saphenous nerve axons *in***
410 ***vivo***

411 In healthy axons, the majority of axonal mitochondria remain stationary regardless of the level of
412 impulse activity. However, stationary mitochondria in electrically stimulated axons are shorter
413 than mitochondria in electrically silent or low frequency conducting axons. This finding has been
414 interpreted as activity-induced mitochondrial fission intended to generate smaller more easily
415 transportable mitochondria (Sajic et al., 2013). To examine the effect of HFD on stationary,
416 polarized mitochondria *in vivo*, we next measured their size by confocal microscopy (Figure 3).
417 There were no differences in the length of stationary mitochondria in young mice fed a short 16-
418 week HFD (4+16) versus control diet (Figures 3A and 3D). However, in mice fed HFD for 36
419 weeks, stationary mitochondria in axons conducting at 1 Hz were significantly *longer* compared
420 to control mice (Figures 3B and 3E). Further, the average size of stationary mitochondria was
421 significantly longer in older mice fed HFD (24+16) versus controls at both frequencies (Figures
422 3C and 3F). To illustrate the change in the size distribution of stationary mitochondria, we
423 stratified the average size data (Figures 3E' and 3F') and presented them as a proportion of all
424 stationary axonal mitochondria (Figures 3B' and 3C'). A trend towards a greater proportion of
425 larger (*i.e.*, longer than 5 μm) versus shorter stationary mitochondria was found in mice fed HFD
426 versus control diet in the 4+36 and 24+16 week groups.

427

428 **HFD fed mice exhibit increased PGC1 α expression in DRGs *in vivo***

429 The transcriptional coactivator PGC1 α is a master regulator of mitochondrial biogenesis, fatty
430 acid oxidation (Scarpulla, 2011), and intracellular calcium levels (Chen et al., 2010). Thus, we
431 next sought to determine whether PGC1 α levels are altered in peripheral nerves of HFD mice.
432 We used confocal fluorescence microscopy to quantify PGC1 α protein expression in spinal cord
433 tissue sections from the lumbar L3 and L4 segments by immunohistochemistry (IHC). The HFD
434 4+36 mice displayed elevated PGC1 α immunoreactivity compared to controls in both L3
435 (Figures 4A-4C) and L4 DRGs (Figures 4D-4F). PGC1 α protein level in lumbar DRG was also
436 significantly increased in HFD versus control mice in a separate cohort fed respective diets from
437 4-36 weeks (Figure 4G). PGC1 α protein level did not differ in HFD versus control sural nerves
438 (Figure 4H). Although PGC1 α can trigger MFN2-mediated mitochondrial fusion, there was no
439 difference in DRG MFN2 protein levels in HFD and control mice (Figure 4-1). VDAC1/2, an
440 important regulator of mitochondrial function, was significantly decreased in HFD sural nerves,
441 but unchanged in HFD DRG (Figure 4-1). Therefore, increased PGC1 α expression occurred
442 concomitantly with increased mitochondrial length (Figure 3), and reduced mitochondrial MMP
443 (Figure 5) and [Ca²⁺]_i in HFD saphenous nerve axons (Figure 7).

444

445 **HFD mice exhibit reduced MMP in saphenous nerve axons *in vivo***

446 MMP is a key requirement for mitochondrial ATP synthesis (Zorova et al., 2018). We showed
447 previously that SFAs decrease MMP in primary DRG neurons *in vitro* (Rumora et al., 2018;
448 Rumora et al., 2019a). Therefore, we next examined whether HFD impaired MMP *in vivo* in
449 axons under conditions of both low and high energy demand. We quantified MMP *in vivo* by
450 acquiring confocal images of TMRM-labeled CFP⁺ axons and calculating the ratio of TMRM
451 intensity in CFP⁺ mitochondria versus TMRM intensity in the adjacent surrounding axoplasm. To
452 monitor MMP within electrically active axons, we imaged saphenous nerve axons while
453 simultaneously stimulating them. In sham-stimulated (*i.e.*, basal energy demand) HFD 4+16 and

454 1 Hz-stimulated (*i.e.*, low energy demand) HFD 4+36 and 24+16 saphenous nerve axons,
455 mitochondria stained more weakly with TMRM than in control mice, indicating lower MMP in
456 HFD mitochondria (Figures 5A, 5A', 5B, and 5C). We next increased axonal energy demand by
457 stimulating the saphenous nerves at 50 Hz, which markedly decreased MMP in control
458 mitochondria (Figures 5B' and 5C'). This is consistent with the basic tenet of mitochondrial
459 function whereby MMP (the proton gradient) is dissipated through complex V to generate ATP.
460 In contrast, in mice fed HFD, conducting at 50 Hz did not change MMP. Overall, this suggests
461 that the lower MMP in HFD mice may suffice to meet basal energy demands for axon survival,
462 but not for meeting the energy demands for the full range of physiological functions, including
463 high frequency impulse activity.

464

465 **HFD mice exhibit impaired axonal conduction in saphenous nerve axons *in vivo***

466 Impulse conduction requires increased ATP production (van Hameren et al., 2019); however,
467 we found herein that HFD mitochondria fail to dissipate MMP in response to electrical
468 stimulation (Figure 5), suggesting that axons from HFD mice may not be able to conduct at the
469 physiological frequencies required for normal functioning, *e.g.*, sensory perception during
470 walking (Prochazka and Gorassini, 1998). Therefore, we examined whether HFD saphenous
471 nerve axons could sustain conduction at physiological frequency *in vivo* by measuring sCAPs,
472 *i.e.*, simultaneous action potentials from several axons. Low frequency (1 Hz) stimulation
473 generated synchronous sCAPs from HFD mice saphenous axons that were comparable to
474 those in control mice (Figure 6-1). Only in some mice on long-term HFD (4+36 weeks) were
475 sCAPs at 1Hz more dispersed, indicating slowing of conduction velocity in some axons (Figure
476 6-1). These findings suggest that even though MMP was significantly lower in HFD versus
477 control axons, HFD mitochondria still generate sufficient ATP to conduct impulses at 1 Hz.
478 Importantly, however, such low level of impulse activity is atypical for non-resting sensory

479 axons, which require sustained impulse conduction between 50 to 150 Hz for moderate physical
480 activity such as walking.

481 Thus, we repeated sCAP recordings during 50 Hz electrical stimulation. In control mice,
482 sCAPs maintained the same shape and amplitude for at least 60 minutes (Figures 6A and 6D);
483 however, sCAP amplitudes steadily declined in both 4+36 (Figures 6B and 6D) and 24+16
484 (Figures 6C and 6D) HFD mice. The reduced sCAP amplitudes were sometimes accompanied
485 by the appearance of additional, late peaks (Figure 6B) and an overall latency increase (Figure
486 6C). The reduced amplitudes during sustained impulse activity were more pronounced in
487 animals fed HFD for a longer period. After 16 weeks of HFD diet, the average sCAP amplitude
488 dropped to $80 \pm 19\%$ [mean \pm standard deviation] of the initial amplitude (Figure 6C'),
489 significantly less than in controls ($p = 0.03$, unpaired Student's t-test). After 36 weeks on HFD,
490 the sCAP amplitudes dropped to as little as only 27% in some animals, with a trending average
491 drop of $71 \pm 34\%$ of the initial amplitude (Figure 6B') ($p = 0.10$, unpaired Student's t-test).

492 To explore the extent of PN in these mice, we next measured their axonal RPT (Smith,
493 1980), a sensitive method for detecting early PN (Braune, 1999). RPT is the period after one
494 action potential has propagated that the axon is refractory to the propagation of a second action
495 potential. We quantified RPT in HFD and control axons by delivering a first stimulus and
496 increasing the delay a second stimulus was applied in steps of 0.1 ms up to a 2.5 ms delay
497 (Figures 6E and 6F). We quantified the percentage of axons that conducted the second stimulus
498 at each stimulus interval (Figures 6G and 6H). In control nerves, some axons were still able to
499 conduct the second stimulus after a delay of only 0.3 ms (Figure 6E, green arrow),
500 approximately 50% still conducted after a 0.8 ms delay, and 80% after a 1.2 ms delay (Figure
501 6H). In contrast, in HFD 24+16 mice, no axons conducted after a 0.3 ms delay, only
502 approximately 10% conducted after a 0.8 ms delay, and about 50% conducted after a 1.2 ms
503 (Figure 6H). These results confirm that 16 weeks on HFD is sufficient to detectably impair

504 conduction. Interestingly, after a longer 36-week HFD duration, RPT tended to revert towards
505 the control pattern (Figure 6G). Nonetheless, these mice showed greater deterioration in their
506 ability to conduct at 50 Hz compared to mice on a shorter diet duration (Figure 6B' and 6C').
507 Overall, our data show that the loss of MMP coincides with the loss of axonal conduction in HFD
508 mice.

509

510 **HFD mice exhibit reduced intra-axonal $[Ca^{2+}]_i$ levels in saphenous nerve axons *in vivo***

511 Since HFD causes axonal mitochondrial deficits, and mitochondria are important regulators of
512 intra-axonal $[Ca^{2+}]_i$ ($[Ca^{2+}]_i$) (Rizzuto et al., 2012), we next examined whether HFD alters $[Ca^{2+}]_i$
513 in saphenous nerve axons *in vivo*. We used the transgenic Tn-XXL mouse, which expresses a
514 calcium-binding troponin C-based biosensor with two fluorescent probes, citrine and CFP (Mank
515 et al., 2008). Calcium binding to the sensor results in fluorescence resonance energy transfer
516 (FRET); thus, $[Ca^{2+}]_i$ can be quantified by taking the ratio of citrine to CFP fluorescence intensity
517 from axons imaged by confocal microscopy (Figures 7A-7C). We first validated our system by
518 incubating saphenous nerve axons *in vivo* in Tn-XXL mice in artificial CSF followed by adding
519 ionomycin, an ionophore that raises $[Ca^{2+}]_i$. As anticipated, the citrine to CFP fluorescence
520 intensity ratio increased (Figure 7D).

521 In preliminary experiments, we examined the consequences of a relatively short duration of
522 HFD (5 weeks) on $[Ca^{2+}]_i$, employing 13-week old Tn-XXL mice (13+5 group). This regimen only
523 caused a moderate body weight increase (22.23 ± 1.13 g in control versus 26.13 ± 0.83 g in
524 HFD), yet, surprisingly, it significantly reduced $[Ca^{2+}]_i$ ($p = 0.0005$, Mann-Whitney test, $n = 4$
525 animals per group, Figure 7C). We examined $[Ca^{2+}]_i$ in HFD 24+16 mice, given that this cohort
526 displayed significantly impaired axonal conduction (Figure 6). This HFD regimen in Tn-XXL mice
527 induced progressive metabolic dysfunction, including accelerated weight gain, hyperglycemia,
528 and glucose intolerance (Figure 7-1), similar to the effects seen in CFP mice (Figure 1).

529 Interestingly, unmyelinated axons (C-fibers, distinguishable by caliber $< 1.5 \mu\text{m}$), which are
530 typically affected early in the course of PN and manifest as pain, showed significantly greater
531 $[\text{Ca}^{2+}]_i$ than larger diameter myelinated axons (4-6 μm) in control mice (Figure 7E). In 24+16
532 HFD Tn-XXL mice, we found a small, but very significant, decrease in $[\text{Ca}^{2+}]_i$ in both myelinated
533 and unmyelinated saphenous nerve axons when compared to Tn-XXL controls (Figure 7F, $p <$
534 0.0001 , unpaired t-test, $n = 9$ animals per group). Taken as a whole, our results show that a 16-
535 week HFD diet caused an unexpected decrease in $[\text{Ca}^{2+}]_i$ *in vivo* in both myelinated and
536 unmyelinated saphenous nerve axons, compared to control mice on control diet.

537

538 **Discussion**

539 PN in prediabetes and T2D exhibits distal-to-proximal nerve damage and axonal dysfunction;
540 however, underlying molecular mechanisms are undefined. Our clinical studies indicate that
541 dyslipidemia, through the metabolic syndrome, contributes to PN, even in normoglycemic
542 individuals (Callaghan et al., 2020). We also reported that long-chain SFAs impair mitochondrial
543 MMP, bioenergetics capacity, ATP production, and motility in cultured DRG neurons (Rumora et
544 al., 2018; Rumora et al., 2019a). Herein, we postulated that similar mechanisms contribute to
545 sensory neuron degeneration *in vivo* during PN. Using a HFD prediabetic mouse model that
546 develops PN (O'Brien et al., 2014) and accumulates ectopic nerve fat (O'Brien et al., 2020), we
547 characterized mitochondrial function within the saphenous nerve, a sensory nerve of bundled
548 axons that relies on mitochondrial axonal trafficking to maintain energy homeostasis (Sajic et
549 al., 2013). Surprisingly, HFD only marginally affected mitochondrial transport; however, it
550 significantly increased stationary mitochondrial size, lowered MMP, and impaired saphenous
551 nerve conduction at physiological frequencies. This suggests that lower MMP in HFD
552 mitochondria may produce insufficient ATP to sustain physiological conduction. Additionally,
553 HFD decreased $[\text{Ca}^{2+}]_i$ and increased DRG PGC1 α expression.

554 We first evaluated whether HFD-feeding has a sex-specific effect on PN. All male and
555 female HFD mice developed metabolic dysfunction and tactile hypersensitivity. Although HFD
556 female mice had delayed onset of tactile hypersensitivity, both sexes exhibited similar tactile
557 responses at 20 and 40 weeks when *in vivo* experiments were conducted. Therefore, the
558 molecular changes underlying PN may not be sex-dependent so we used HFD male mice
559 throughout the study. Male HFD 4+36 mice had elevated plasma cholesterol and phospholipids
560 associated with PN, similar to previous studies (Tesfaye et al., 2005). Alterations in cholesterol
561 level (Madamanchi and Runge, 2007) and phospholipid composition (Lu and Claypool, 2015)
562 are reported to compromise mitochondrial function in dyslipidemia models, so we evaluated the
563 effect of HFD on mitochondrial events *in vivo*.

564 We anticipated HFD-induced mitochondrial transport deficiencies *in vivo* in saphenous nerve
565 based on our *in vitro* data (Rumora et al., 2018); however, no significant differences were
566 observed. Indeed, short-term HFD increased motile mitochondria numbers in young mice, but
567 not in old mice. The response to short-term HFD in young mice may represent a compensatory
568 mechanism to counteract partial MMP loss and impaired energy production (Baqri et al., 2009),
569 which may fail in old animals. In young mice, healthy polarized mitochondria are rapidly
570 transported into areas of localized, experimentally-induced saphenous nerve axon damage to
571 avert local bioenergetics collapse (Sajic et al., 2018). The discrepancy between our *in vitro* and
572 *in vivo* results perhaps reflects myelination state, which is absent *in vitro* but present around
573 many saphenous axons *in vivo* (Ohno et al., 2011).

574 We found that HFD significantly increased the average mitochondrial size *in vivo*, indicating
575 a shift towards mitochondrial biogenesis. Similar to PGC1 α -overexpressing cardiac myocytes
576 (Russell et al., 2004), we observed increased PGC1 α protein levels in HFD DRG that correlated
577 with increases in mitochondrial size. Since PGC1 α stimulates fatty acid oxidation (Scarpulla,
578 2011; Cheng et al., 2018), higher PGC1 α levels in HFD DRGs may be a compensatory

579 mechanism to boost mitochondrial biogenesis and offset MMP loss and energy deficits (Zhang
580 et al., 2019). PGC1 α can also induce mitochondrial fusion by activating MFN2 (Zorzano, 2009).
581 However, as seen in skeletal muscle (Jheng et al., 2012) and hepatic tissue (Lionetti et al.,
582 2014), we found no change in DRG and sural MFN2 protein levels, suggesting that
583 mitochondrial fusion is not responsible for the HFD-induced increases in axonal mitochondrial
584 size in sensory nerves. PGC1 α also regulates mitochondrial metabolism and apoptosis through
585 VDAC1/2 (Shoshan-Barmatz et al., 2010; Gill et al., 2019). Indeed, we found a significant
586 decrease in VDAC1/2 protein expression in HFD sensory nerves. Therefore, increased DRG
587 PGC1 α expression may not be sufficient to offset mitochondrial energy deficits in the sensory
588 nerve axons resulting in a loss of VDAC1/2 expression indicative of mitochondrial dysfunction.

589 *In vitro*, SFAs decreased MMP in DRG neurons (Rumora et al., 2018; Rumora et al., 2019a;
590 Rumora et al., 2019b), and HFD exerted a similar effect *in vivo*, even after short-term HFD.
591 Similarly, SFAs decreased MMP in C2C12 mouse muscle cells (Jheng et al., 2012) and primary
592 mouse cardiomyocytes (Joseph et al., 2016). The partial MMP loss we measured in HFD mouse
593 saphenous mitochondria didn't completely abrogate axonal function. This suggests that
594 elevated SFAs in the HFD reduce MMP by partially uncoupling the proton gradient from ATP
595 production in the saphenous nerve. Partial uncoupling of the proton gradient allows more
596 electron carriers (NADH/FADH₂) to enter the electron transport chain, thereby increasing fatty
597 acid β -oxidation and ATP production to sustain axonal function (Skulachev, 1998; Hinder et al.,
598 2019). However, increased energy demand may result in a complete loss of MMP and energy
599 production within HFD saphenous nerves. Therefore, at low energy demand, the HFD
600 saphenous nerve conducted; however, increasing demand to 50 Hz simulation, levels
601 commensurate with daily activities, e.g., walking (Prochazka and Gorassini, 1998), prompted
602 limited conduction, suggesting inability to supply additional ATP for impulse conduction. This
603 progressive conduction slowing/blocking likewise precedes overt PN in diabetics (Dyck et al.,

604 2005). Moreover, further MMP reductions may completely depolarize axonal mitochondria,
605 triggering degradation, and chronic ATP shortages might increase intra-axonal Na^+ levels,
606 causing axonal degeneration (Stys et al., 1992). Conversely, healthy saphenous axons from
607 control mice readily conducted at 50 Hz, as expected since MMP drives ATP synthesis (Nicholls
608 and Ferguson, 2013). Indeed, impulse conduction in healthy saphenous nerve coincides with
609 increased ATP production (van Hameren et al., 2019). Our study is the first, to our knowledge,
610 to quantify MMP changes in adult mammalian axons during impulse conduction *in vivo*. The
611 partial dissipation of MMP may be an important step to increase ATP synthesis during impulse
612 conduction.

613 Saphenous nerve MMP and axonal conduction were impaired even though distal axonal
614 terminals were structurally intact in the hairy skin they innervate on the medial foot dorsum,
615 supporting human studies demonstrating conduction defects before PN onset (Dyck et al.,
616 2005). HFD animals developed PN in glabrous skin on the plantar foot innervated by the sciatic
617 nerve, evidenced by lower IENFD compared to controls. This result is supported by studies
618 evaluating effects of 45-60% HFD in prediabetic mice on glabrous skin, which exhibit IENFD
619 loss as a PN marker (Vincent et al., 2009; Rumora et al., 2019b; O'Brien et al., 2020). The
620 differential impact of HFD on IENFD in glabrous versus hairy skin may reflect effects of
621 increased body weight on the plantar foot in HFD mice (Collongues et al., 2018).

622 Importantly, we found lower saphenous axonal $[\text{Ca}^{2+}]_i$ in HFD mice versus controls before
623 overt PN. SFAs increase $[\text{Ca}^{2+}]_i$ at the expense of endoplasmic reticulum Ca^{2+} stores, prompting
624 excessive intra-mitochondrial Ca^{2+} in T2D models (Ly et al., 2017). Palmitate raises $[\text{Ca}^{2+}]_i$ in
625 mouse (Remizov et al., 2003) and human (Gwiazda et al., 2009) primary β -cells, rat INS-1
626 insulinoma cells (Schnell et al., 2007), and mouse podocytes (Xu et al., 2015), and elevated
627 $[\text{Ca}^{2+}]_i$ is a unifying axonal degeneration mechanism across multiple neuronal injury types
628 (LoPachin and Lehning, 1997), including diabetic PN (Ferryhough and Calcutt, 2010). DRGs

629 from streptozotocin-induced type 1 diabetes and genetic leptin signaling-deficient *db/db* T2D
630 mice exhibit elevated $[Ca^{2+}]_i$ (Kostyuk et al., 1999); however, shorter diabetes durations induced
631 no discernible effects (Kostyuk et al., 2001), suggesting calcium dyshomeostasis occurs early.
632 Thus, lower $[Ca^{2+}]_i$ may be an earlier pathological consequence of metabolic disturbance and
633 higher $[Ca^{2+}]_i$ likely occurs during later irreversible stages of PN.

634 Our study had several limitations. First, although we did not find sex differences in the
635 development of metabolic dysfunction or tactile hypersensitivity, there may be sex dimorphism
636 in mitochondrial activity *in vivo* in response to the HFD. Future studies will assess the effect of
637 HFD on MMP, $[Ca^{2+}]_i$, and PGC1 α expression in the saphenous nerve from female and male
638 mice. Second, we identified an early decrease in axonal $[Ca^{2+}]_i$ before overt PN in HFD mice,
639 suggesting that decreased axonal $[Ca^{2+}]_i$ is an early pathological response to metabolic
640 dysfunction and that axonal $[Ca^{2+}]_i$ may increase in later-stage PN pathogenesis. Although we
641 did not test this hypothesis herein, future studies will focus on calcium flux in saphenous nerve
642 axons. Although low number of biological replicates is a study limitation, we observed replicable
643 and significant results. Future studies will focus on increasing the number of mice for sCAP
644 analyses and axonal $[Ca^{2+}]_i$ assessment, to reduce variance between animals.

645 Our findings lend new insight into early pathological events in saphenous nerve axons
646 underlying PN development during HFD-induced prediabetes. MMP reduction was a key
647 pathogenic event and may consequently reduce the ability of mitochondria to increase ATP
648 production to meet energy demands, which is relevant to daily activities, like sensory perception
649 during walking. Impairment of mitochondrial function also associated with several compensatory
650 mechanisms, including increased mitochondrial size and transport and elevated PGC1 α
651 expression. Importantly, these mechanisms were accompanied by reduced $[Ca^{2+}]_i$, which may
652 have profound consequences for axonal signaling, maintenance, and regeneration. We suggest
653 that diminished MMP in HFD mitochondria creates unbalanced axonal energy supply and

654 demand concomitant with decreased axonal $[Ca^{2+}]_i$, thereby contributing to PN progression in
655 prediabetes.

656 **References**

- 657 Baqri RM, Turner BA, Rheuben MB, Hammond BD, Kaguni LS, Miller KE (2009) Disruption
658 of mitochondrial DNA replication in *Drosophila* increases mitochondrial fast axonal
659 transport in vivo. *PLoS One* 4:e7874.
- 660 Braune HJ (1999) Testing of the refractory period in sensory nerve fibres is the most sensitive
661 method to assess beginning polyneuropathy in diabetics. *Electromyogr Clin Neurophysiol*
662 39:355-359.
- 663 Callaghan BC, Little AA, Feldman EL, Hughes RA (2012) Enhanced glucose control for
664 preventing and treating diabetic neuropathy. *Cochrane Database Syst Rev*:CD007543.
- 665 Callaghan BC, Xia R, Reynolds E, Banerjee M, Rothberg AE, Burant CF, Villegas-Umana E,
666 Pop-Busui R, Feldman EL (2016a) Association Between Metabolic Syndrome
667 Components and Polyneuropathy in an Obese Population. *JAMA Neurol* 73:1468-1476.
- 668 Callaghan BC, Gao L, Li Y, Zhou X, Reynolds E, Banerjee M, Pop-Busui R, Feldman EL, Ji L
669 (2018) Diabetes and obesity are the main metabolic drivers of peripheral neuropathy.
670 *Ann Clin Transl Neurol* 5:397-405.
- 671 Callaghan BC, Reynolds EL, Banerjee M, Chant E, Villegas-Umana E, Gardner TW, Votruba K,
672 Giordani B, Pop-Busui R, Pennathur S, Feldman EL (2020) The Prevalence and
673 Determinants of Cognitive Deficits and Traditional Diabetic Complications in the
674 Severely Obese. *Diabetes Care*.
- 675 Callaghan BC, Xia R, Banerjee M, de Rekeneire N, Harris TB, Newman AB, Satterfield S,
676 Schwartz AV, Vinik AI, Feldman EL, Strotmeyer ES, Health ABCS (2016b) Metabolic
677 Syndrome Components Are Associated With Symptomatic Polyneuropathy Independent
678 of Glycemic Status. *Diabetes Care* 39:801-807.
- 679 Chada SR, Hollenbeck PJ (2004) Nerve growth factor signaling regulates motility and docking
680 of axonal mitochondria. *Curr Biol* 14:1272-1276.
- 681 Chen M, Wang Y, Qu A (2010) PGC-1 alpha accelerates cytosolic Ca²⁺ clearance without
682 disturbing Ca²⁺ homeostasis in cardiac myocytes. *Biochem Biophys Res Commun*
683 396:894-900.
- 684 Cheng CF, Ku HC, Lin H (2018) PGC-1 α as a Pivotal Factor in Lipid and Metabolic Regulation.
685 *Int J Mol Sci* 19.
- 686 Collongues N, Samama B, Schmidt-Mutter C, Chamard-Witkowski L, Debouverie M, Chanson
687 JB, Antal MC, Benardais K, de Seze J, Velten M, Boehm N (2018) Quantitative and
688 qualitative normative dataset for intraepidermal nerve fibers using skin biopsy. *PLoS One*
689 13:e0191614.
- 690 Dyck PJ, O'Brien PC, Litchy WJ, Harper CM, Klein CJ (2005) Monotonicity of nerve tests in
691 diabetes: subclinical nerve dysfunction precedes diagnosis of polyneuropathy. *Diabetes*
692 *Care* 28:2192-2200.
- 693 Eid S, Sas KM, Abcouwer SF, Feldman EL, Gardner TW, Pennathur S, Fort PE (2019) New
694 insights into the mechanisms of diabetic complications: role of lipids and lipid
695 metabolism. *Diabetologia* 62:1539-1549.
- 696 Feldman EL, Callaghan BC, Pop-Busui R, Zochodne DW, Wright DE, Bennett DL, Bril V,
697 Russell JW, Viswanathan V (2019) Diabetic neuropathy. *Nat Rev Dis Primers* 5:41.
- 698 Fernyhough P, Calcutt NA (2010) Abnormal calcium homeostasis in peripheral neuropathies.
699 *Cell Calcium* 47:130-139.
- 700 Gill JF, Delezie J, Santos G, McGuirk S, Schnyder S, Frank S, Rausch M, St-Pierre J, Handschin
701 C (2019) Peroxisome proliferator-activated receptor γ coactivator 1 α regulates

- 702 mitochondrial calcium homeostasis, sarcoplasmic reticulum stress, and cell death to
703 mitigate skeletal muscle aging. *Aging Cell* 18:e12993.
- 704 Gwiazda KS, Yang TL, Lin Y, Johnson JD (2009) Effects of palmitate on ER and cytosolic
705 Ca²⁺ homeostasis in beta-cells. *Am J Physiol Endocrinol Metab* 296:E690-701.
- 706 Hinder LM, Sas KM, O'Brien PD, Backus C, Kayampilly P, Hayes JM, Lin CM, Zhang H,
707 Shanmugam S, Rumora AE, Abcouwer SF, Brosius FC, 3rd, Pennathur S, Feldman EL
708 (2019) Mitochondrial uncoupling has no effect on microvascular complications in type 2
709 diabetes. *Sci Rep* 9:881.
- 710 Jheng HF, Tsai PJ, Guo SM, Kuo LH, Chang CS, Su IJ, Chang CR, Tsai YS (2012)
711 Mitochondrial fission contributes to mitochondrial dysfunction and insulin resistance in
712 skeletal muscle. *Mol Cell Biol* 32:309-319.
- 713 Joseph LC, Barca E, Subramanyam P, Komrowski M, Pajvani U, Colecraft HM, Hirano M,
714 Morrow JP (2016) Inhibition of NADPH Oxidase 2 (NOX2) Prevents Oxidative Stress
715 and Mitochondrial Abnormalities Caused by Saturated Fat in Cardiomyocytes. *PLoS One*
716 11:e0145750.
- 717 Kostyuk E, Svichar N, Shishkin V, Kostyuk P (1999) Role of mitochondrial dysfunction in
718 calcium signalling alterations in dorsal root ganglion neurons of mice with
719 experimentally-induced diabetes. *Neuroscience* 90:535-541.
- 720 Kostyuk E, Voitenko N, Kruglikov I, Shmigol A, Shishkin V, Efimov A, Kostyuk P (2001)
721 Diabetes-induced changes in calcium homeostasis and the effects of calcium channel
722 blockers in rat and mice nociceptive neurons. *Diabetologia* 44:1302-1309.
- 723 Lionetti L, Mollica MP, Donizzetti I, Gifuni G, Sica R, Pignalosa A, Cavaliere G, Gaita M, De
724 Filippo C, Zorzano A, Putti R (2014) High-lard and high-fish-oil diets differ in their
725 effects on function and dynamic behaviour of rat hepatic mitochondria. *PLoS One*
726 9:e92753.
- 727 LoPachin RM, Lehning EJ (1997) Mechanism of calcium entry during axon injury and
728 degeneration. *Toxicol Appl Pharmacol* 143:233-244.
- 729 Lu YW, Claypool SM (2015) Disorders of phospholipid metabolism: an emerging class of
730 mitochondrial disease due to defects in nuclear genes. *Front Genet* 6:3.
- 731 Ly LD, Xu S, Choi SK, Ha CM, Thoudam T, Cha SK, Wiederkehr A, Wollheim CB, Lee IK,
732 Park KS (2017) Oxidative stress and calcium dysregulation by palmitate in type 2
733 diabetes. *Experimental & molecular medicine* 49:e291.
- 734 Madamanchi NR, Runge MS (2007) Mitochondrial dysfunction in atherosclerosis. *Circ Res*
735 100:460-473.
- 736 Mank M, Santos AF, Drenberger S, Mrcic-Flogel TD, Hofer SB, Stein V, Hendel T, Reiff DF,
737 Levelt C, Borst A, Bonhoeffer T, Hubener M, Griesbeck O (2008) A genetically encoded
738 calcium indicator for chronic in vivo two-photon imaging. *Nat Methods* 5:805-811.
- 739 Morris RL, Hollenbeck PJ (1993) The regulation of bidirectional mitochondrial transport is
740 coordinated with axonal outgrowth. *J Cell Sci* 104 (Pt 3):917-927.
- 741 Nicholls DG, Ferguson SJ (2013) 5 - Respiratory Chains. In: *Bioenergetics (Fourth Edition)*
742 (Nicholls DG, Ferguson SJ, eds), pp 91-157. Boston: Academic Press.
- 743 O'Brien PD, Sakowski SA, Feldman EL (2014) Mouse models of diabetic neuropathy. *ILAR*
744 *journal* 54:259-272.
- 745 O'Brien PD, Guo K, Eid SA, Rumora AE, Hinder LM, Hayes JM, Mendelson FE, Hur J,
746 Feldman EL (2020) Integrated lipidomic and transcriptomic analyses identify altered

- 747 nerve triglycerides in mouse models of prediabetes and type 2 diabetes. *Dis Model Mech*
748 13.
- 749 Obrosova IG, Ilynska O, Lyzogubov VV, Pavlov IA, Mashtalir N, Nadler JL, Drel VR (2007)
750 High-fat diet induced neuropathy of pre-diabetes and obesity: effects of "healthy" diet
751 and aldose reductase inhibition. *Diabetes* 56:2598-2608.
- 752 Ohno N, Kidd GJ, Mahad D, Kiryu-Seo S, Avishai A, Komuro H, Trapp BD (2011) Myelination
753 and axonal electrical activity modulate the distribution and motility of mitochondria at
754 CNS nodes of Ranvier. *The Journal of neuroscience : the official journal of the Society*
755 *for Neuroscience* 31:7249-7258.
- 756 Prochazka A, Gorassini M (1998) Models of ensemble firing of muscle spindle afferents
757 recorded during normal locomotion in cats. *J Physiol* 507 (Pt 1):277-291.
- 758 Remizov O, Jakubov R, Dufer M, Krippeit Drews P, Drews G, Waring M, Brabant G,
759 Wienbergen A, Rustenbeck I, Schofl C (2003) Palmitate-induced Ca²⁺-signaling in
760 pancreatic beta-cells. *Molecular and cellular endocrinology* 212:1-9.
- 761 Rizzuto R, De Stefani D, Raffaello A, Mammucari C (2012) Mitochondria as sensors and
762 regulators of calcium signalling. *Nat Rev Mol Cell Biol* 13:566-578.
- 763 Rumora AE, LoGrasso G, Haidar JA, Dolkowski JJ, Lentz SI, Feldman EL (2019a) Chain length
764 of saturated fatty acids regulates mitochondrial trafficking and function in sensory
765 neurons. *Journal of lipid research* 60:58-70.
- 766 Rumora AE, Lentz SI, Hinder LM, Jackson SW, Valesano A, Levinson GE, Feldman EL (2018)
767 Dyslipidemia impairs mitochondrial trafficking and function in sensory neurons. *FASEB*
768 *journal : official publication of the Federation of American Societies for Experimental*
769 *Biology* 32:195-207.
- 770 Rumora AE, LoGrasso G, Hayes JM, Mendelson FE, Tabbey MA, Haidar JA, Lentz SI, Feldman
771 EL (2019b) The Divergent Roles of Dietary Saturated and Monounsaturated Fatty Acids
772 on Nerve Function in Murine Models of Obesity. *The Journal of neuroscience : the*
773 *official journal of the Society for Neuroscience* 39:3770-3781.
- 774 Russell LK, Mansfield CM, Lehman JJ, Kovacs A, Courtois M, Saffitz JE, Medeiros DM,
775 Valencik ML, McDonald JA, Kelly DP (2004) Cardiac-specific induction of the
776 transcriptional coactivator peroxisome proliferator-activated receptor gamma coactivator-
777 1alpha promotes mitochondrial biogenesis and reversible cardiomyopathy in a
778 developmental stage-dependent manner. *Circ Res* 94:525-533.
- 779 Saeedi P, Petersohn I, Salpea P, Malanda B, Karuranga S, Unwin N, Colagiuri S, Guariguata L,
780 Motala AA, Ogurtsova K, Shaw JE, Bright D, Williams R (2019) Global and regional
781 diabetes prevalence estimates for 2019 and projections for 2030 and 2045: Results from
782 the International Diabetes Federation Diabetes Atlas, 9(th) edition. *Diabetes Res Clin*
783 *Pract* 157:107843.
- 784 Sajic M (2014) Mitochondrial dynamics in peripheral neuropathies. *Antioxidants & redox*
785 *signaling* 21:601-620.
- 786 Sajic M, Ida KK, Canning R, Gregson NA, Duchon MR, Smith KJ (2018) Mitochondrial damage
787 and "plugging" of transport selectively in myelinated, small-diameter axons are major
788 early events in peripheral neuroinflammation. *Journal of neuroinflammation* 15:61.
- 789 Sajic M, Mastrolia V, Lee CY, Trigo D, Sadeghian M, Mosley AJ, Gregson NA, Duchon MR,
790 Smith KJ (2013) Impulse conduction increases mitochondrial transport in adult
791 mammalian peripheral nerves in vivo. *PLoS Biol* 11:e1001754.

- 792 Savelieff MG, Callaghan BC, Feldman EL (2020) The emerging role of dyslipidemia in diabetic
793 microvascular complications. *Curr Opin Endocrinol Diabetes Obes* 27:115-123.
- 794 Scarpulla RC (2011) Metabolic control of mitochondrial biogenesis through the PGC-1 family
795 regulatory network. *Biochimica et biophysica acta* 1813:1269-1278.
- 796 Schnell S, Schaefer M, Schofl C (2007) Free fatty acids increase cytosolic free calcium and
797 stimulate insulin secretion from beta-cells through activation of GPR40. *Molecular and*
798 *cellular endocrinology* 263:173-180.
- 799 Schonfeld P, Wojtczak L (2016) Short- and medium-chain fatty acids in energy metabolism: the
800 cellular perspective. *Journal of lipid research* 57:943-954.
- 801 Shoshan-Barmatz V, De Pinto V, Zweckstetter M, Raviv Z, Keinan N, Arbel N (2010) VDAC, a
802 multi-functional mitochondrial protein regulating cell life and death. *Mol Aspects Med*
803 31:227-285.
- 804 Skulachev VP (1998) Uncoupling: new approaches to an old problem of bioenergetics.
805 *Biochimica et biophysica acta* 1363:100-124.
- 806 Smith KJ (1980) A sensitive method for the detection and quantification of conduction deficits in
807 nerve. *J Neurol Sci* 48:191-199.
- 808 Stys PK, Waxman SG, Ransom BR (1992) Ionic mechanisms of anoxic injury in mammalian
809 CNS white matter: role of Na⁺ channels and Na⁽⁺⁾-Ca²⁺ exchanger. *The Journal of*
810 *neuroscience : the official journal of the Society for Neuroscience* 12:430-439.
- 811 Tesfaye S, Chaturvedi N, Eaton SE, Ward JD, Manes C, Ionescu-Tirgoviste C, Witte DR, Fuller
812 JH, Group EPCS (2005) Vascular risk factors and diabetic neuropathy. *N Engl J Med*
813 352:341-350.
- 814 van Hameren G, Campbell G, Deck M, Berthelot J, Gautier B, Quintana P, Chrast R, Tricaud N
815 (2019) In vivo real-time dynamics of ATP and ROS production in axonal mitochondria
816 show decoupling in mouse models of peripheral neuropathies. *Acta Neuropathol*
817 *Commun* 7:86.
- 818 Vincent AM, Hayes JM, McLean LL, Vivekanandan-Giri A, Pennathur S, Feldman EL (2009)
819 Dyslipidemia-induced neuropathy in mice: the role of oxLDL/LOX-1. *Diabetes* 58:2376-
820 2385.
- 821 Vincent AM, Edwards JL, McLean LL, Hong Y, Cerri F, Lopez I, Quattrini A, Feldman EL
822 (2010) Mitochondrial biogenesis and fission in axons in cell culture and animal models of
823 diabetic neuropathy. *Acta Neuropathol* 120:477-489.
- 824 Xu S, Nam SM, Kim JH, Das R, Choi SK, Nguyen TT, Quan X, Choi SJ, Chung CH, Lee EY,
825 Lee IK, Wiederkehr A, Wollheim CB, Cha SK, Park KS (2015) Palmitate induces ER
826 calcium depletion and apoptosis in mouse podocytes subsequent to mitochondrial
827 oxidative stress. *Cell death & disease* 6:e1976.
- 828 Zhang CL, Ho PL, Kintner DB, Sun D, Chiu SY (2010) Activity-dependent regulation of
829 mitochondrial motility by calcium and Na/K-ATPase at nodes of Ranvier of myelinated
830 nerves. *The Journal of neuroscience : the official journal of the Society for Neuroscience*
831 30:3555-3566.
- 832 Zhang Q, Lei YH, Zhou JP, Hou YY, Wan Z, Wang HL, Meng H (2019) Role of PGC-1 α in
833 Mitochondrial Quality Control in Neurodegenerative Diseases. *Neurochem Res* 44:2031-
834 2043.
- 835 Zorova LD, Popkov VA, Plotnikov EY, Silachev DN, Pevzner IB, Jankauskas SS, Babenko VA,
836 Zorov SD, Balakireva AV, Juhaszova M, Sollott SJ, Zorov DB (2018) Mitochondrial
837 membrane potential. *Anal Biochem* 552:50-59.

838 Zorzano A (2009) Regulation of mitofusin-2 expression in skeletal muscle. *Appl Physiol Nutr*
839 *Metab* 34:433-439.

840 **Figures legends**

841 **Figure 1. HFD mice exhibit weight gain and impaired glucose tolerance typical of**
842 **prediabetes**

843 (Top) Scheme of the three experimental groups: (i) mice fed HFD from 4 weeks of age for 16
844 weeks (4+16 weeks), (ii) mice fed HFD from 4 weeks of age for 36 weeks (4+36 weeks), and
845 (iii) mice fed HFD from 24 weeks of age for 16 weeks (24+16 weeks). The control diet and HFD
846 fatty acid composition is provided in Figure 1-1 (Extended data). Respective control mice
847 received control chow. At the endpoint, mitochondrial transport and morphology, and axonal
848 $[Ca^{2+}]_i$, were measured *in vivo* along with electrophysiological measurements. (A-B) HFD 4+16
849 and 4+36 mice gain more weight than their respective controls and the percentage weight
850 increase is significant starting from 15 and 19 weeks of HFD, respectively, and onwards ($p <$
851 0.001 , 2-way ANOVA, $n = 5-28$ animals per time point). (C) HFD 24+16 mice gain more weight
852 than their respective controls and the percentage weight increase is significant starting from 3
853 weeks of HFD and onwards ($p < 0.001$, 2-way ANOVA, $n = 3-10$ animals per time point). (A')
854 Terminal fasting blood glucose (FBG) at the experiment endpoint in HFD 4+16 mice was not
855 significantly different to the controls ($n = 5$ control, $n = 8$ HFD). (B') Terminal FBG in HFD 4+36
856 mice was significantly higher than the controls (** $p < 0.01$, unpaired 2-tailed Student's t-test, $n =$
857 10 control, $n = 7$ HFD). (C') Terminal FBG in HFD 24+36 mice was significantly higher than the
858 controls (* $p < 0.05$, unpaired 2-tailed Student's t-test, $n = 8$ control, $n = 7$ HFD). The impact of
859 HFD on food consumption, FBG, body weight, and tactile response in male and female mice is
860 shown in Figure 1-2 (Extended data). (A'') Intraperitoneal glucose tolerance test (ipGTT) in HFD
861 4+16 mice was significantly different to controls at all time points (* $p < 0.05$, ** $p < 0.01$, *** $p <$
862 0.001 , Bonferroni post-hoc test, $n = 4-5$ per group). The overall effect from the HFD diet was
863 extremely significant ($p < 0.0001$, 2-way ANOVA). (B'') ipGTT in HFD 4+36 mice was

864 significantly different to controls at 60 and 120 min (**p < 0.001, Bonferroni post-hoc test, n = 4-
865 7 per group). The overall effect from the HFD diet was extremely significant (p < 0.0001, 2-way
866 ANOVA). (C'') ipGTT in HFD 24+16 mice was significantly different to controls at 30, 60, and
867 120 min (**p < 0.001, Bonferroni post-hoc test, n = 10 per group). The overall effect from the
868 HFD diet was extremely significant (p < 0.0001, 2-way ANOVA). (D) Plasma cholesterol levels
869 were significantly increased in HFD versus control 4+36 mice (****p < 0.0001, 1-way ANOVA, n
870 = 3 per group). (E) Plasma phospholipid levels were significantly increased in HFD versus
871 control 4+36 mice (****p < 0.0001, 1-way ANOVA, n = 3 per group). (F) Non-esterified fatty acid
872 (NEFA) levels did not differ in HFD versus control 4+36 mice (1-way ANOVA, n = 3 per group).
873 (G) Triglyceride levels did not differ in HFD versus control 4+36 mice (1-way ANOVA, n = 3 per
874 group). Quantitation of hairy skin and glabrous skin IENFD is shown in Figure 1-3 (Extended
875 data).

876 SEM, standard error of the mean.

877

878 **Figure 2. HFD mice do not exhibit impaired mitochondrial transport in saphenous nerve**
879 **axons *in vivo***

880 (A) The saphenous nerve (black arrow), blood vessels, and the surrounding connective and fat
881 tissue are exposed in the left thigh after skin incision. Scale bar = 1 cm. (B) Time-lapse high
882 magnification confocal image of saphenous nerve axons in CFP transgenic mouse with CFP⁺
883 axonal mitochondria (blue). Isolectin-IB4 (green) labels a proportion of unmyelinated C-fibers
884 and tetramethylrhodamine methyl ester (TMRM) labels polarized mitochondria (CFP⁺, TMRM⁺
885 mitochondria are magenta, pink, or white; CFP⁻, TMRM⁺ mitochondria are red). Scale bar = 50
886 μm. (C) Spider-web diagram showing characteristics of polarized, motile mitochondria in sham-
887 stimulated saphenous nerve axons of HFD 4+16 mice. There were significantly more motile
888 anterograde and retrograde mitochondria in HFD than in control axons (*p < 0.05, 2-way

889 ANOVA, data represent mean of 37-66 axons per group for each category analyzed, n = 2 mice
890 per group). Videos of mitochondrial trafficking in control diet and HFD mice are shown in Movies
891 1 and 2 respectively. (D-E) Spider-web diagrams showing characteristics of polarized, motile
892 mitochondria in stimulated saphenous nerve axons of 4+36 (D) or 24+16 (E) mice. There were
893 no overall differences in axonal mitochondrial transport. However, HFD 4+36 mice exhibited
894 larger anterogradely transported mitochondria in nerves conducting at 50 Hz and higher
895 average retrograde speed at 1 Hz (*p < 0.05, 2-way ANOVA, data represent mean of 77-97 total
896 axons per group, n = 3 mice per group). HFD 24+16 mice exhibited larger average speed of
897 anterograde mitochondrial transport at both 1 and 50 Hz and higher anterograde maximum
898 speed of mitochondrial transport at only 1 Hz (**p < 0.01, 2-way ANOVA, data represent mean
899 of 77-97 total axons per group, n = 3 mice per group).

900

901 **Figure 3. HFD mice exhibit increased stationary mitochondrial size in saphenous nerve**
902 **axons *in vivo***

903 (A-C and A'-C') High magnification confocal image of saphenous nerve axons in CFP transgenic
904 mouse with CFP⁺ axonal mitochondria (blue) stimulated at 1 Hz. TMRM labels polarized
905 mitochondria; CFP⁺, TMRM⁺ mitochondria are magenta, pink, or white; CFP⁻, TMRM⁺
906 mitochondria are red. Scale bar = 10 μm. (A-C) In saphenous nerve from control 4+16 (A), 4+36
907 (B), and 24+16 (C) mice. (A'-C') In saphenous nerve axons from HFD 4+16 (A'), 4+36 (B') and
908 24+16 (C') mice. Several axonal mitochondria were longer in older HFD (white arrows) than in
909 control mice. (D) HFD 4+16 mice had similar average stationary mitochondrial size at the
910 experiment endpoint in their saphenous nerve axons compared to controls (mean ± SEM, n = 2
911 mice per group, n = 2996 control mitochondria, n = 9987 HFD mitochondria). (E-F) HFD 4+36
912 and 24+16 mice had increased average stationary mitochondrial size at the experiment
913 endpoint in their saphenous nerve axons stimulated at 1 Hz and for HFD 24+16 mice also at 50

914 Hz versus controls (* $p < 0.05$, *** $p < 0.001$, 2-way ANOVA, mean \pm SEM, $n = 4-5$ mice per
915 group). (E'-F') Distribution of stationary mitochondrial size at the experiment endpoint in
916 saphenous nerve axons shows a shift towards larger mitochondria in 4+36 and 24+16 HFD
917 versus control mice.

918 CI, confidence interval; SEM, standard error of the mean.

919

920 **Figure 4. HFD fed mice exhibit increased PGC1 α expression in lumbar DRG *in vivo***

921 (A-B) Representative, flattened Z-stack confocal image of a L3 section from control and HFD
922 4+36 mice, labeled by IHC with anti-PGC1 α antibody (red) and counterstained with DAPI.

923 Punctate PGC1 α labeling is noticeable in several DRGs (white arrows), particularly in HFD
924 mice. Scale bar = 10 μm . (C) Quantification of percent area labeled with anti-PGC1 α antibody in

925 L3 tissue shows significant increase in PGC1 α expression in HFD versus control mice (*** $p <$
926 0.001, Mann-Whitney test median [25%-75% percentile]: HFD 3.96 [3.2-6.5] versus control 1.75

927 [0.9-2.5], $n = 5$ mice per group). (D-E) Representative, flattened Z-stack confocal image of a L4
928 section from control or HFD 4+36 mice, labeled by IHC with anti-PGC1 α antibody (red) and

929 counterstained with DAPI. Punctate PGC1 α staining is noticeable in several DRGs. Scale bar =
930 10 μm . (F) Quantification of percent area labeled with anti-PGC1 α antibody in L4 tissue shows

931 significant increase in PGC1 α expression in HFD versus control mice (* $p < 0.05$, Mann-Whitney
932 test, median [25%-75% percentile]: control 2.7 [1.6-5.3] versus HFD 4.5 [2.2-7.3], $n = 5$ mice per

933 group). (G) Western blot analysis of right and left L1-L5 lumbar DRG shows a significant

934 increase in PGC1 α protein level in HFD versus control mice at 36 weeks of age (* $p < 0.05$, t-

935 tailed unpaired t-test, $n = 8-9$ mice per group). (H) Western blot analysis of sural nerves shows

936 no change in PGC1 α protein level in HFD versus control mice at 36 weeks of age (t-tailed

937 unpaired t-test, n = 9-10 mice per group). Western blot analysis of MFN2 and VDAC1/2 protein
938 level in DRG and sural sensory nerve is shown in Figure 4-1 (Extended data).

939 CTRL, control; DRG, dorsal root ganglion; HFD, high-fat diet; IQR, interquartile range.

940

941 **Figure 5. HFD mice exhibit reduced MMP in saphenous nerve axons *in vivo***

942 (A-C) High magnification confocal image of saphenous nerve axons in CFP transgenic mouse
943 with CFP⁺ axonal mitochondria (blue, top panel) stimulated at 1 Hz. TMRM labels polarized
944 mitochondria (red, middle panel). Bottom panel is merged; CFP⁺, TMRM⁺ mitochondria are
945 magenta, pink, or white; CFP⁻, TMRM⁺ mitochondria are red. In control mice, all axonal
946 mitochondria were polarized and were either magenta, pink, or white on merged images
947 (bottom; red mitochondria are either axonal, non-CFP expressing or non-axonal). In contrast, in
948 all HFD groups, some axonal mitochondria were depolarized and appear blue on merged
949 images (bottom, white arrows). (A') The ratio of TMRM intensity in CFP⁺ mitochondria versus
950 the adjacent axoplasm indicates MMP and is significantly lower in HFD 4+16 mice versus
951 controls (**p < 0.001, unpaired Student's t-test, mean ± SEM, n = 4-5 mice per group). (B') The
952 ratio of TMRM intensity in CFP⁺ mitochondria versus the adjacent axoplasm indicates MMP and
953 is significantly lower in HFD 4+36 mice versus controls in 1 Hz-stimulated axons. Increasing the
954 stimulation frequency to 50 Hz lowers MMP in control mitochondria but has no effect in HFD
955 mitochondria (*p < 0.05, **p < 0.01, ***p < 0.001, 2-way ANOVA, mean ± SEM, n = 4-5 mice per
956 group). (C') The ratio of TMRM intensity in CFP⁺ mitochondria versus the adjacent axoplasm
957 indicates MMP and is significantly lower in HFD 24+16 mice versus controls in axons stimulated
958 at 1 Hz. Increasing the stimulation frequency to 50 Hz lowers MMP in control mitochondria but
959 has no effect in HFD mitochondria (*p < 0.05, **p < 0.01, ***p < 0.001, 2-way ANOVA, mean ±
960 SEM, n = 4-5 mice per group).

961 IQR, interquartile range; SEM, standard error of the mean.

962

963 **Figure 6. HFD mice exhibit impaired axonal conduction in saphenous nerve axons *in vivo***

964 (A) Waterfall graph of sCAPs from a control mouse, which remain relatively unchanged over 1

965 hour of sustained impulse activity at 50 Hz. The earliest records are at the front of this plot and

966 all other waterfall plots. (B) Waterfall graph of sCAPs from a 4+36 HFD mouse, which

967 progressively change over 1 hour of sustained impulse activity at 50 Hz. The records show a

968 loss of amplitude over time and the labile appearance of axons conducting at longer latency.

969 (B') Plot of change in sCAP amplitude after 1 hour of conducting at 50 Hz, expressed as a

970 percentage of the starting amplitude. There is no mean loss of amplitude in controls, but a mean

971 reduction of 29% in HFD 4+36 mice ($p = 0.05$, unpaired Student's t-test, $n = 3$ control, $n = 5$

972 HFD). Example traces of conduction at 1 Hz in HFD and control 4+36 mice are shown in Figure

973 6-1 (Extended data). (C) Waterfall graph of sCAPs from a 24+16 HFD mouse, which

974 progressively change over 1 hour of sustained impulse activity at 50 Hz. The records show a

975 loss of amplitude, indicative of conduction block or partial depolarization, and increase in

976 latency, indicating conduction slowing. (C') Plot of change in sCAP amplitude after 1 hour of

977 conducting at 50 Hz, expressed as a percentage of the starting amplitude. There is no mean

978 loss of amplitude in controls, but a mean reduction of 20% in HFD 24+16 mice ($p = 0.03$,

979 unpaired Student's t-test, $n = 3$ control, $n = 6$ HFD). (D) Loss of sCAP amplitude over time in a

980 control (green), 4+36 HFD (dark red), and 24+16 HFD (red) mouse, showing dramatic loss in %

981 of axons conducting 50 Hz in HFD mice. (E) Waterfall graph of RPTs in a control mouse,

982 revealing that a proportion of axons can still conduct a second stimulus delivered 0.3 ms after

983 the first (green arrow); the proportion of axons that conduct the second stimulus increases as

984 the interval increases. (F) Waterfall graph of RPTs in a HFD 24+16 mouse, revealing, in

985 contrast to controls (E), axons require at least a 0.8 ms interval before they can conduct the

986 second stimulus (red arrow). (G) Graph comparing RPT recovery in control (green) and HFD
987 (red) 4+36 mice, expressed as the recovery in amplitude of the second as a proportion of the
988 first sCAP, is similar between the control and HFD 4+36 mice. (H) Graph comparing RPT
989 recovery in control (green) and HFD (red) 24+16 mice, expressed as the recovery in amplitude
990 of the second as a proportion of the first sCAP, is significantly prolonged in HFD versus control
991 mice (**p < 0.01, 2-way ANOVA, n = 3 control, n = 6 HFD). This shows impaired ability of HFD
992 axons to conduct closely spaced impulses.

993

994 **Figure 7. HFD mice exhibit reduced intra-axonal [Ca²⁺]_i levels in saphenous nerve axons**
995 ***in vivo***

996 (A) Confocal image of an exposed saphenous nerve *in vivo* in a Tn-XXL mouse. Scale bar =
997 400 μm. (B-C) High magnification confocal image in CFP, citrine, and citrine FRET channels
998 with a merge of CFP and citrine FRET, of saphenous nerve axons bathed *in vivo* with artificial
999 CSF (ACSF) (B) or ionomycin (100 μM) for 20 minutes (C). Scale bar = 50 μm. (D) Citrine to
1000 CFP intensity ratio increases after incubating control Tn-XXL mouse saphenous nerve axons in
1001 ionomycin (100 μM) for 20 minutes (n = 4 mice per group, n = 257-318 axons per group). (E)
1002 Pilot data of HFD 9+5 mice exhibit reduced [Ca²⁺]_i in myelinated axons compared to controls (*p
1003 < 0.05, Mann-Whitney test, mean ± SEM, n = 4 control mice with n = 318 axons, n = 4 HFD
1004 mice with n = 148 axons). (F) HFD 24+16 mice exhibit reduced [Ca²⁺]_i in both myelinated and
1005 unmyelinated fibers compared to controls (**p < 0.01, ***p < 0.001, Kruskal-Wallis test, mean ±
1006 SEM, n = 9 control mice with n = 70 axons, n = 10 HFD mice with n = 60 axons). Weight gain
1007 and impaired glucose tolerance in Tn-XXL (calcium reporter) mice is shown in Figure 7-1
1008 (Extended data).

1009 SEM, standard error of the mean.

1010

1011

1012 **Extended data files:**

1013 **Figure 1-1. Fatty acid composition of the control diet and 45% high-fat diets.**

1014 The protein, carbohydrate, and fat content in the control diet (Lab Diets, catalog # 5001) and
1015 45% HFD (Research Diets, catalog # D12451) is provided along with the percentage of
1016 saturated, monounsaturated, and polyunsaturated fatty acids in each diet.

1017

1018 **Figure 1-2. Male and female mice exhibit similar metabolic and neuropathy phenotypes.**

1019 (A) All male and female HFD and control (CTRL) mice consumed around 4 g of food per day.
1020 (B) Fasting blood glucose was significantly increased to approximately 8 mmol/L in HFD versus
1021 control mice, regardless of sex. (C) Male and female HFD mice gained weight throughout the
1022 study. Female HFD mice gained a significantly higher percent weight between 22-26 weeks of
1023 age compared to male HFD mice. (D-E) A von Frey test was used to measure tactile sensitivity
1024 of HFD and control mice to calibrated filaments. Male HFD mice exhibited tactile hypersensitivity
1025 between 24-28 weeks of age while female HFD mice developed tactile hypersensitivity at 32
1026 weeks of age. * $p < 0.05$, ** $p < 0.01$, *** $p < 0.001$, 2-way ANOVA with Bonferroni's multiple
1027 comparison. CTRL, control; HFD, high-fat diet.

1028

1029 **Figure 1-3. HFD mice do not exhibit IENFD loss in the hairy skin innervated by the**
1030 **saphenous nerve but do show IENFD loss in the glabrous skin innervated by sciatic**
1031 **nerve.**

1032 (A-B) Left panel: Confocal images of hairy skin labeled with anti- β -III-tubulin (red) to visualize
1033 saphenous nerve axonal terminals (white arrows). Right panel: Quantification of epidermal skin
1034 layer area labeled with anti- β -III-tubulin showed no differences in IENFD in HFD 24+16 (A) or
1035 4+36 (B) versus control mice. (C-D) Left panel: Confocal images of glabrous skin labeled with
1036 anti- β -III-tubulin (red) to visualize saphenous nerve axonal terminals. Right panel: Quantification
1037 of the epidermal skin layer area labeled with anti- β -III-tubulin showed a significant reduction in
1038 IENFD in HFD 24+16 (C) or 4+36 (D) versus control mice, $p < 0.0001$, Mann-Whitney test.
1039 IENFD, intraepidermal nerve fiber density, GSK, glabrous skin; HSK, hairy skin.

1040

1041 **Movie 1. Time-lapse video of axonal mitochondrial trafficking in a control mouse *in vivo***
1042 **in saphenous nerve conducting at 1 Hz.** High magnification, time-lapse confocal image of
1043 saphenous nerve axons in a control 24+16 CFP transgenic mouse with CFP+ axonal
1044 mitochondria (blue) stimulated at 1 Hz. TMRM labels polarized mitochondria, CFP+, TMRM+,
1045 which are magenta, pink, or white (blue arrow). CFP-, TMRM+ Schwann cell mitochondria are
1046 red (white arrow). Relative to the imaging site, axons were stimulated at 1 Hz proximally (left of
1047 the image) and conducted compound action potentials were recorded distally (right of the
1048 image). Many motile mitochondria move in either direction. A node of Ranvier is present in the
1049 upper part of the image (yellow arrowhead). Scale bar = 10 μ m.

1050

1051 **Movie 2. Time-lapse video of axonal mitochondrial trafficking in a HFD mouse *in vivo* in**
1052 **saphenous nerve conducting at 50 Hz.** High magnification, time-lapse confocal image of
1053 saphenous nerve axons in a control 24+16 CFP transgenic mouse with CFP+ axonal
1054 mitochondria (blue) stimulated at 50 Hz. TMRM labels polarized mitochondria, CFP+, TMRM+,
1055 which are magenta, pink, or white (blue arrow). CFP-, TMRM+ Schwann cell mitochondria are

1056 red (white arrow). Relative to the imaging site, axons were stimulated at 50 Hz proximally (left of
1057 the image) and conducted compound action potentials were recorded distally (right of the
1058 image). Many motile mitochondria move in either direction. A node of Ranvier is present in the
1059 upper part of the image (yellow arrowhead). Scale bar = 10 μ m.

1060 **Figure 4-1. MFN2 and VDAC1/2 expression in HFD versus control mice in DRG and sural**
1061 **nerves *in vivo***

1062 (A-B) Western blot analysis of L1-L5 lumbar DRG (A) and sural nerves (B) shows no change in
1063 MFN2 protein level in HFD versus control mice at 36 weeks of age (2-tailed unpaired t-test, n =
1064 9-10 mice per group). (C) Western blot analysis of right and left L1-L5 lumbar DRG shows no
1065 change in VDAC1/2 protein level in HFD versus control mice at 36 weeks of age (2-tailed
1066 unpaired t-test, n = 7-8 mice per group). (D) Western blot analysis of sural nerves shows a
1067 significant decrease in VDAC1/2 protein level in HFD versus control mice at 36 weeks of age (*p
1068 < 0.05, 2-tailed unpaired t-test, n = 9 mice per group).

1069

1070 **Figure 6-1. Example traces of conduction at 1 Hz in HFD and control 4+36 mice.**

1071 (A) Typical size and shape of sensory compound action potential (sCAP) recorded from
1072 saphenous nerve in control mice. (B) Most HFD 4+36 mice exhibited similar sCAP size, shape,
1073 and latency as control mice. (C) Some HFD 4+36 mice exhibited delayed and dispersed sCAP,
1074 with smaller amplitude compared with control mice.

1075

1076 **Figure 7-1. Tn-XXL (calcium reporter) mice exhibit pronounced weight gain and impaired**
1077 **glucose tolerance typical of prediabetes.**

1078 (A) Tn-XXL 24+16 HFD mice gain more weight than their respective controls and the
1079 percentage weight increase is significant starting from 3 weeks of HFD and onwards (*p <

1080 0.001, 2-way ANOVA, n = 9 for control group, n=10 for HFD group). (B) Terminal fasting blood
1081 glucose in Tn-XXL 24+16 HFD mice was significantly different to the controls (*p = 0.03, Mann-
1082 Whitney test, n = 9 control group, n = 10 HFD group). (C) Intraperitoneal glucose tolerance test
1083 in Tn-XXL 24+16 HFD mice was significantly different to controls at 30, 60, and 120 min (**p <
1084 0.01, ****p < 0.0001, Bonferroni post-hoc test, n = 9 control group, n = 10 HFD group). The
1085 overall effect from the diet was significant (p < 0.001, 2-way ANOVA).

1086

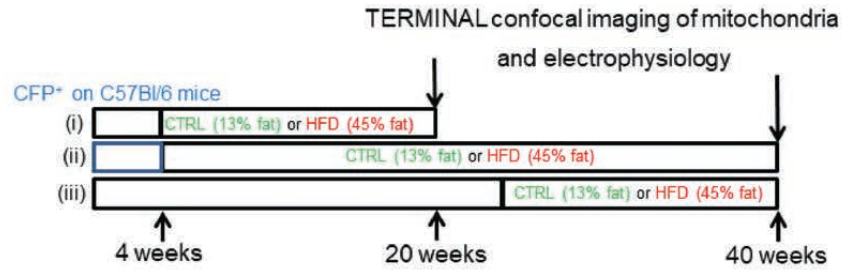
1087

1088

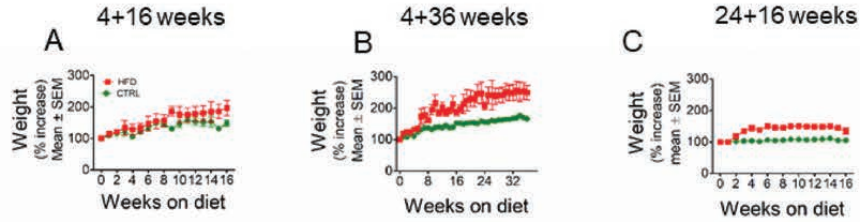
1089

1090

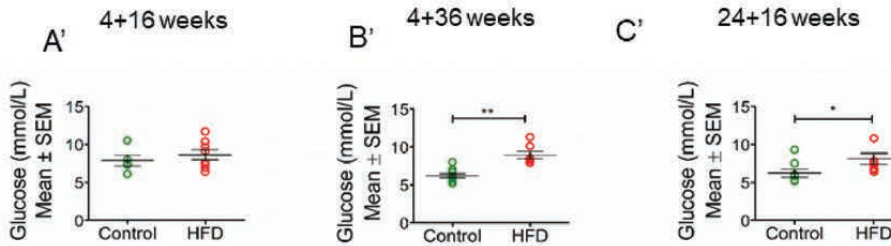
1091



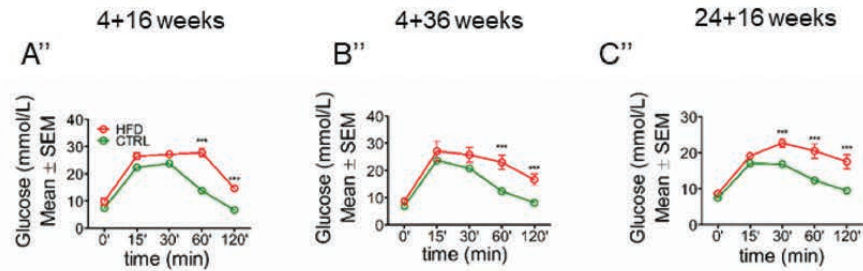
WEIGHT



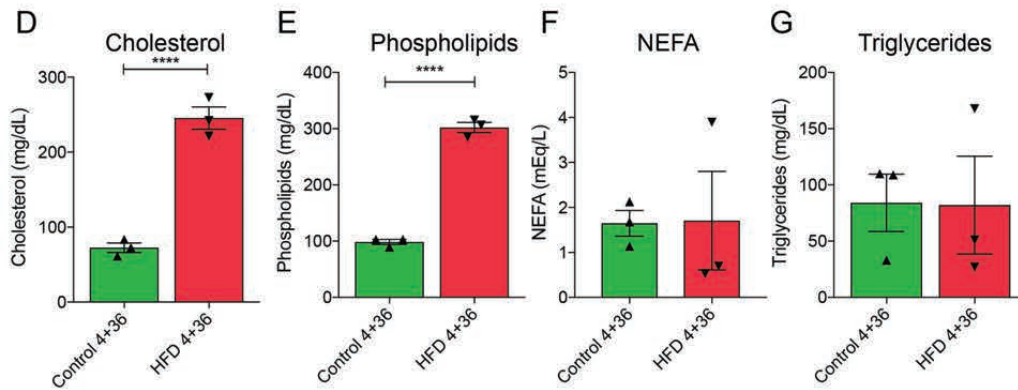
TERMINAL FASTING GLUCOSE

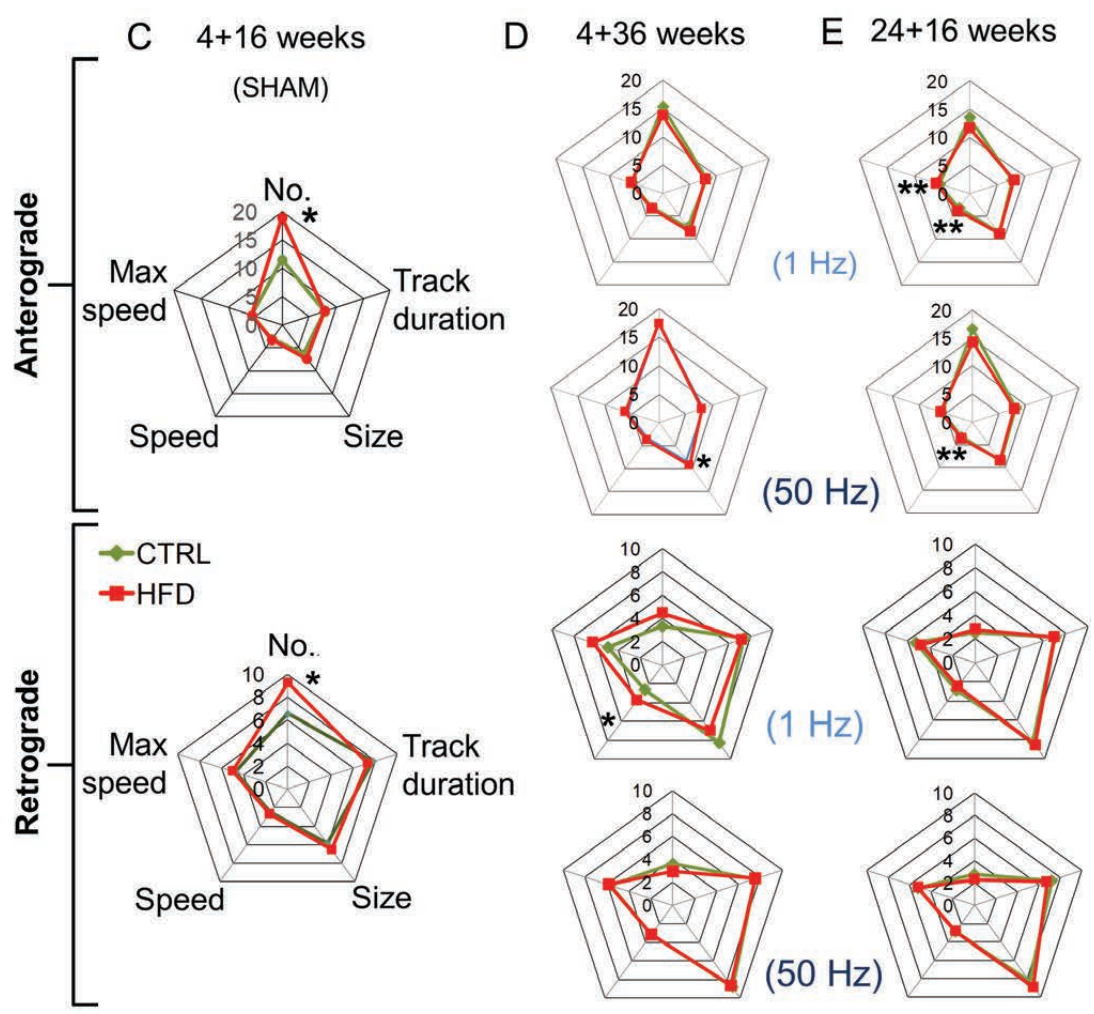
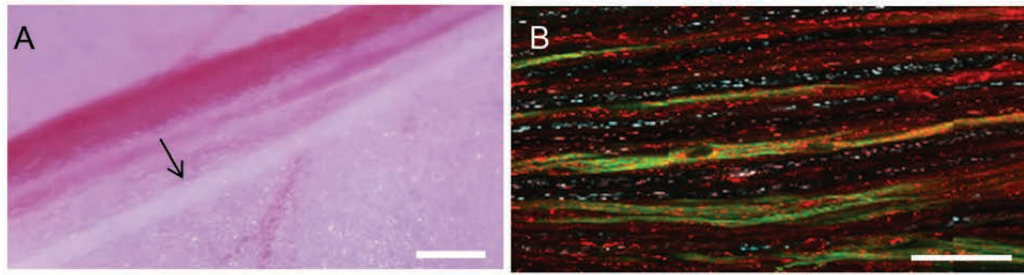


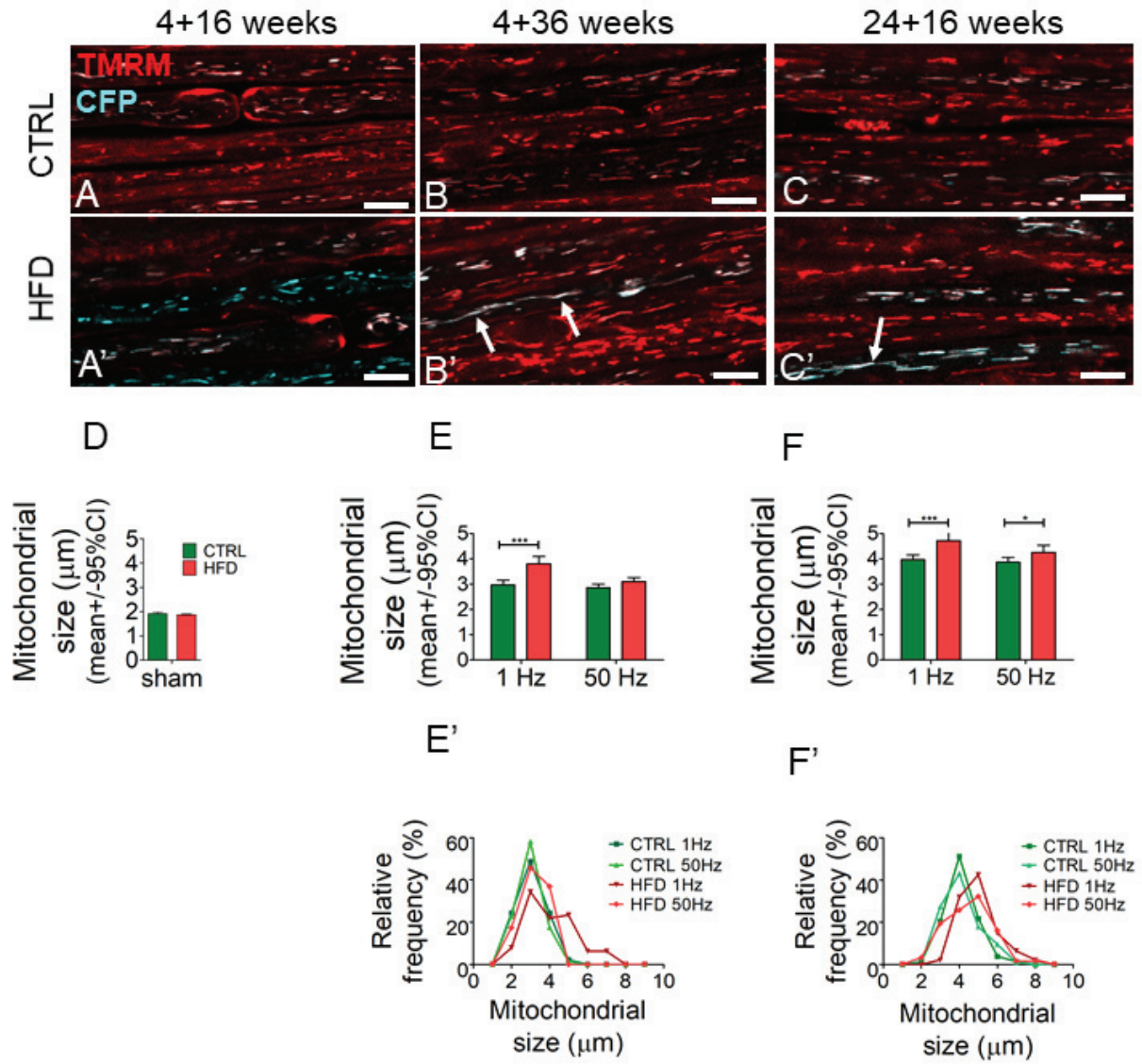
TERMINAL IPGTT

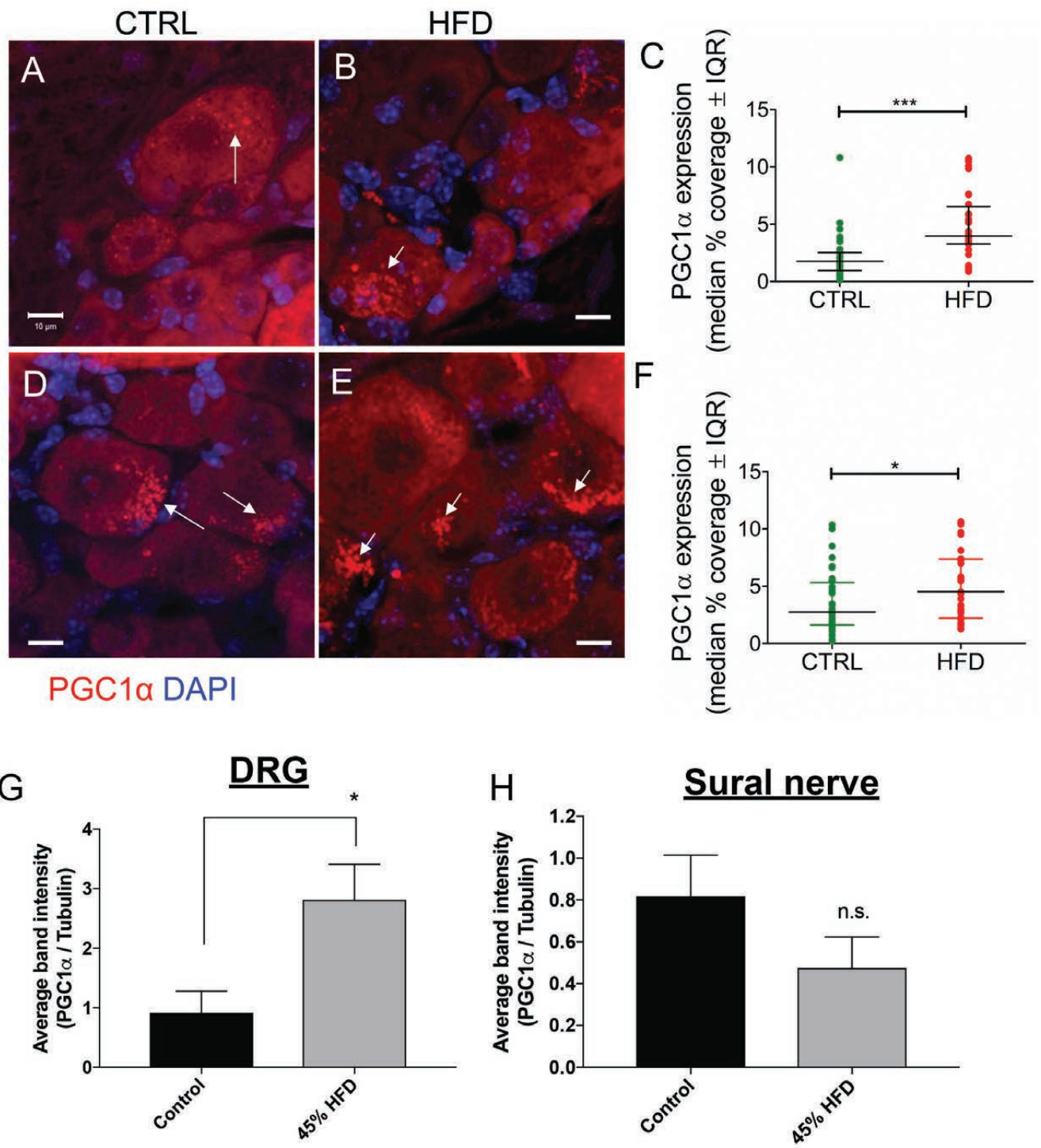


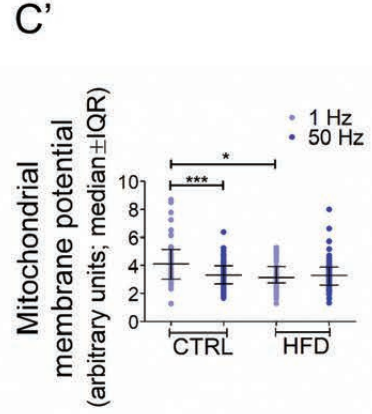
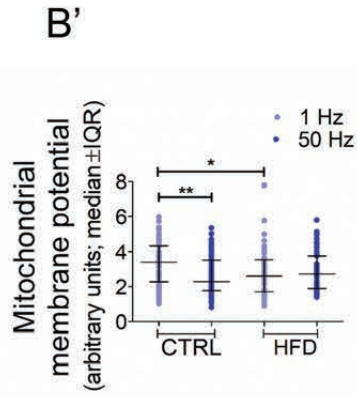
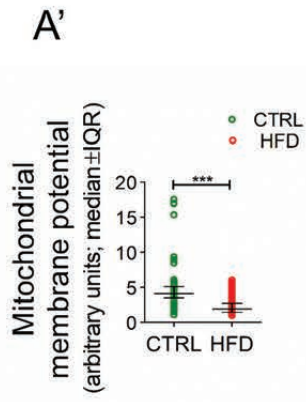
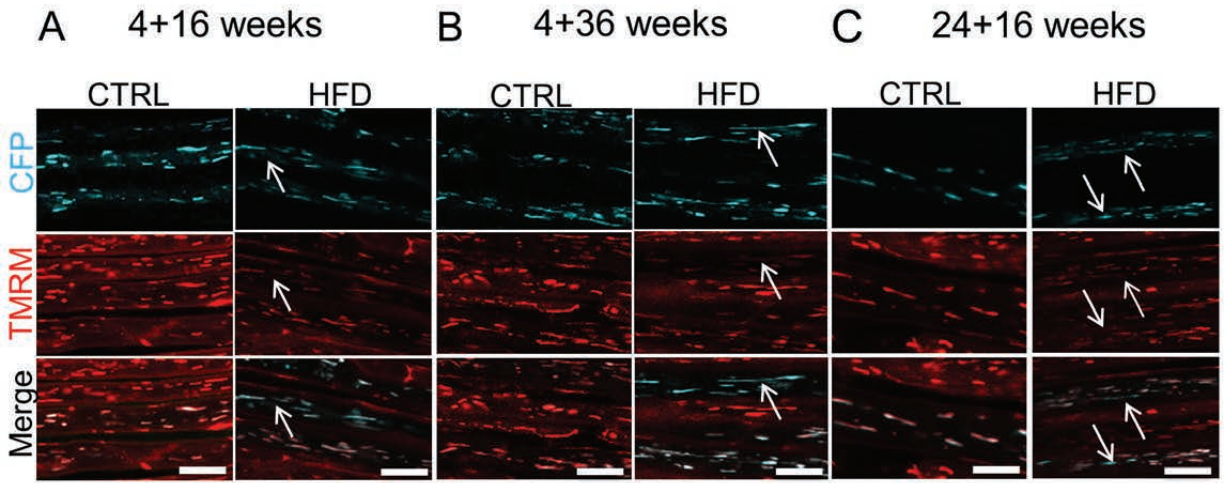
PLASMA LIPID LEVELS



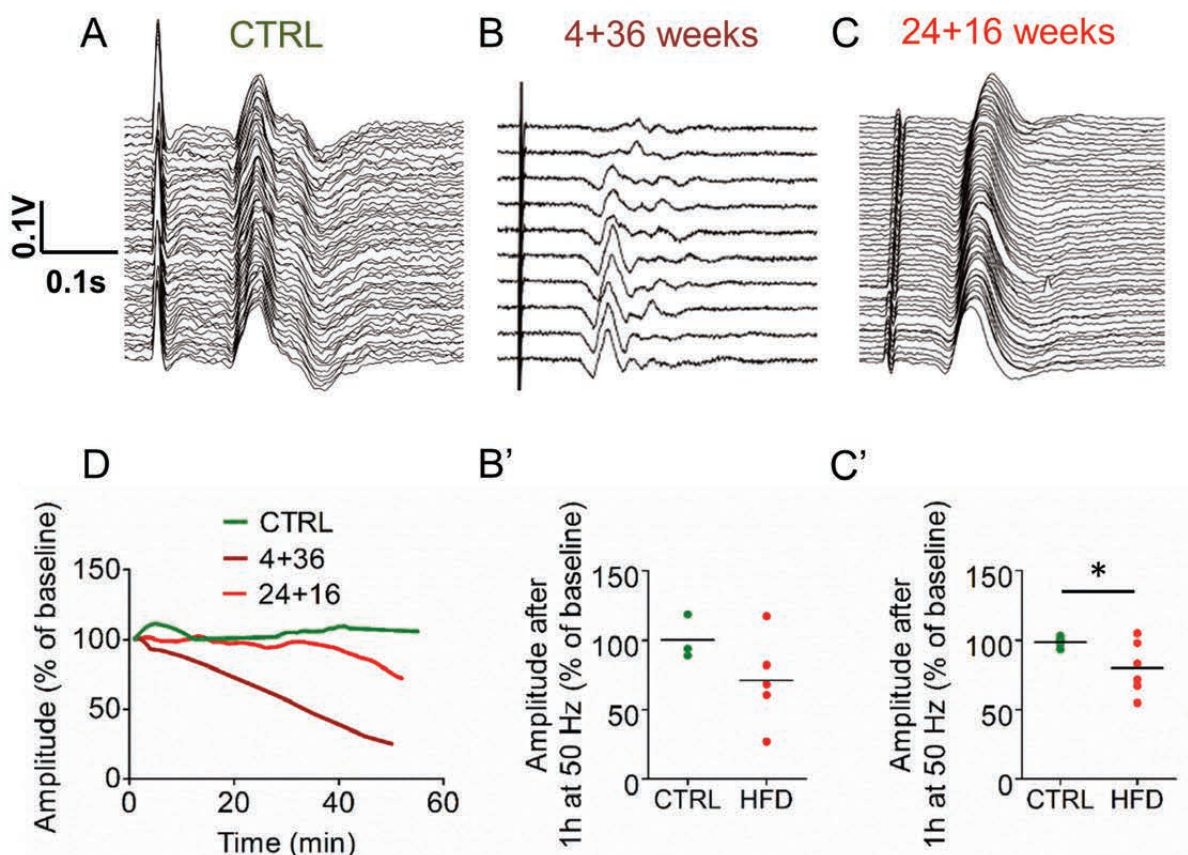








50 Hz conduction for 1 hour



Refractory period

